IOWA STATE UNIVERSITY
Digital Repository

Retrospective Theses and Dissertations

Iowa State University Capstones, Theses and Dissertations

1996

Application of imaging techniques for characterizing MPI data

Atul Subhash Athavale
Iowa State University

Follow this and additional works at: https://lib.dr.iastate.edu/rtd

 Part of the Electrical and Computer Engineering Commons

Recommended Citation
Athavale, Atul Subhash, "Application of imaging techniques for characterizing MPI data" (1996). *Retrospective Theses and Dissertations*. 116.
https://lib.dr.iastate.edu/rtd/116

This Thesis is brought to you for free and open access by the Iowa State University Capstones, Theses and Dissertations at Iowa State University Digital Repository. It has been accepted for inclusion in Retrospective Theses and Dissertations by an authorized administrator of Iowa State University Digital Repository. For more information, please contact digirep@iastate.edu.

www.manaraa.com

Application of imaging techniques for characterizing MPI data

by

Atul Subhash Athavale

A thesis submitted to the graduate faculty

in partial fulfillment of the requirements for the degree of

MASTER OF SCIENCE

Department: Electrical and Computer Engineering

Major: Electrical Engineering

Major Professor: Lalita Udpa

Iowa State University

Ames, Iowa

1996

Copyright © Atul Subhash Athavale, 1996. All rights reserved.

Graduate College

Iowa State University

This is to certify that the Master's thesis of

Atul Subhash Athavale

has met the thesis requirements of Iowa State University

TABLE OF CONTENTS

ACKNOWLEDGMENTS

I wish to express my sincere gratitude to my advisor Dr. Lalita Udpa for providing guidance and invaluable help for this research. It has been my privilege to work with Dr. Lalita Udpa. I wish to thank my committee members for their support and suggestions in preparing this thesis. I am also thankful to other graduate students and researchers in the NDE group at Iowa State University for their assistance. This work was supported by a graduate research assistantship provided by NIST.

ABSTRACT

The Magnetic particle inspection (MPI) method is widely used in the industry for detecting surface or near surface flaws in ferromagnetic specimens. However, the attempts to quantify the physics underlying the method have been limited. This thesis is an effort to model the behavior of the magnetic particles under the influence of magnetic leakage fields. Imaging techniques are used to recreate the dynamics of the particles prior to their reaching an equilibrium around the flaw. The proposed approach has the capability to predict the time to equilibrium of the magnetic particles. Furthermore, the efficiency of the MPI method in terms of the fraction of the total number of particles around the flaw and the signal to noise ratio of the MPI image is predicted. The overall model can be used to obtain forward transfer functions between the flaw depth; and the time to equilibrium, efficiency and signal to noise ratio of the MPI image. Optimal experimental conditions for flaws of different depths are predicted.

CHAPTER 1. INTRODUCTION

Motivation

Non-destructive evaluation (NDE) is defined as the testing of a specimen for flaws without physical harm to the specimen. In recent years a lot of emphasis has been placed on the use of NDE techniques for better quality control. Industries which use NDE methods on a large scale include rail-roads, steel industry, aircraft industry, nuclear industry, gas pipeline inspections etc.

A variety of NDE methods have been developed over the years to address a large range of applications. Ultrasonic, radiographic and electromagnetic methods have emerged as the most dominant of the NDE methods. These methods differ from each other in the form of input energy to the NDE system. A generic NDE system consists of the major components shown in Figure 1.1 [18].

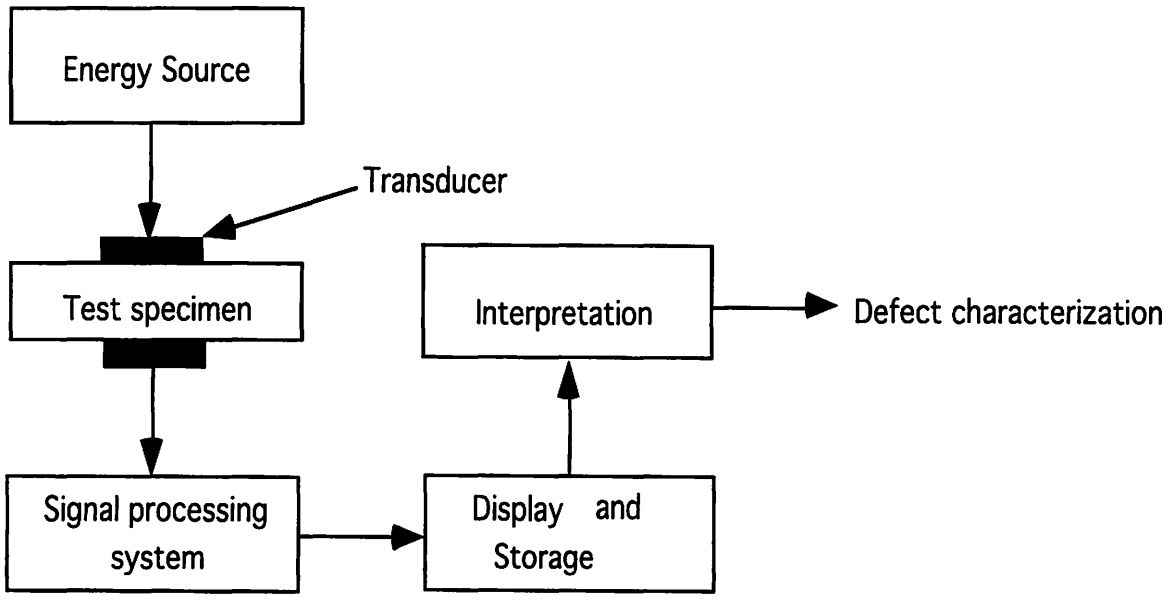

Figure 1.1. A generic NDE system

Acoustic waves are the source of excitation in ultrasonic methods, X-rays are used in radiographic methods and electromagnetic waves are used in electromagnetic methods. Electromagnetic NDE methods have become extremely popular in heavy metal industries because of the sensitivity of metals to electromagnetic energy in the entire spectrum. The magnetic flux leakage (MFL) method is especially popular as an NDE tool for ferromagnetic and paramagnetic specimens. In principle this method consists of magnetizing the test part which serves to set up a leakage field in the presence of discontinuities. The leakage field is detected by scanning the surface of the specimen by flux sensitive sensors. The sensors could be lumped or distributed. A common example of lumped sensors is a Hall probe while that of distributed sensors are magnetic particles. The magnetic particle inspection (MPI) method derives its name from the use of the magnetic particles as sensors for the magnetic flux leakage phenomena.

The MPI method was developed in the early 1920s and the first patent in this field was issued to Major William E. Hoke of the US Army in 1922 [4]. However this method was commercialized by Alfred Victor De Forest in 1929. He formed Magnaflux Corporation in 1934 which became a world leader in MPI test equipment.

Even though the MPI technique had been widely used since 1934, the probability of detection [14] [17] of a flaw using this method remained as low as 50 percent until the 1980s [4]. This was largely due to the fact that it was a qualitative method, attributed in part to the lack of quantitative modeling efforts. Even today the modeling efforts in this area remain limited. This study attempts to give a new thrust to this area by using imaging techniques to model the underlying physics. Imaging techniques are used to recreate the dynamics of the particles prior to their reaching an equilibrium around a flaw. The proposed approach has the capability to predict the time to equilibrium of the magnetic particles. Furthermore, the efficiency of the method in terms of the fraction of the total number of particles around the flaw and the signal to noise ratio of the MPI image is predicted. The overall model can be used

to obtain forward transfer functions between the flaw depth; and the time to equilibrium, efficiency and signal to noise ratio of the MPI image. Optimal experimental conditions for flaws of different depths is predicted.

Organization of this study

This study begins with a discussion of various electromagnetic NDE methods including the MFL method, the eddy current NDE method and the microwave NDE method. This is followed by detailed explanation of the various aspects of an MPI test. The MPI simulation model is then developed including the stochastic distribution of the magnetic particles on the surface of the specimen, the prediction of the leakage fields using finite element analysis, and a quantitative formula for calculating the force on the magnetic particles. This model is then simulated to display MPI images and define parameters for an optimal MPI test. Concluding remarks and recommendations are proposed in the final chapter.

CHAPTER 2. ELECTROMAGNETIC NDE METHODS

Introduction

Nondestructive evaluation (NDE) techniques are typically classified based on the type of the probing energy source [18]. Some of the popular NDE techniques include ultrasonic, radiographic and electromagnetic techniques. Electromagnetic techniques use electric and magnetic fields as the source of input energy. These inspection modalities are used most effectively in gas pipelines, railroads and other industries involving the use of metals due to the sensitivity of metals to energy in the electromagnetic spectrum. Some of the more popular electromagnetic techniques include magnetic flux leakage (MFL) methods, eddy current methods and microwave methods. The primary difference between these methods is the frequency of the input energy. The MFL methods use a frequency of zero, eddy current methods use low input frequencies while microwave methods use high input frequencies in the order of several GHz. This chapter gives an overview of these techniques explaining the fundamental principles underlying each method.

Magnetic flux leakage NDE methods

The Magnetic Flux Leakage (MFL) NDE methods are based on magnetizing the ferromagnetic test specimen and scanning its surface with a flux sensitive sensor. The effectiveness of this method for ferromagnetic specimens is due to their material structure. In these materials there exist domains each of which have a strong magnetic moment. However under ordinary circumstances, the domains are randomly aligned so that the bulk magnetization of the specimen is zero. In the presence of an external magnetic field, the domains experience a rotational torque which alignes them to the magnetic field. In addition, the domains already in the direction of the magnetic field expand at the cost of other domains. Thus there exists a strong magnetic field within these specimens. Also when the magnetic

field is removed, the specimen retains some of its magnetism giving rise to a phenomenon called hysteresis. In the presence of any non-ferromagnetic discontinuity the change in the internal field is significant. This causes the detection of the flaw.

There are two types of MFL methods viz. active and residual. The active method is based on the operation of the test specimen on the initial magnetization curve while the residual method is based on its operation along the demagnetization curve.

Active MFL method

The physics of this method can be explained by considering a rectangular bar which is magnetized by injecting a current along its long axis. The rectangular bar has a rectangular

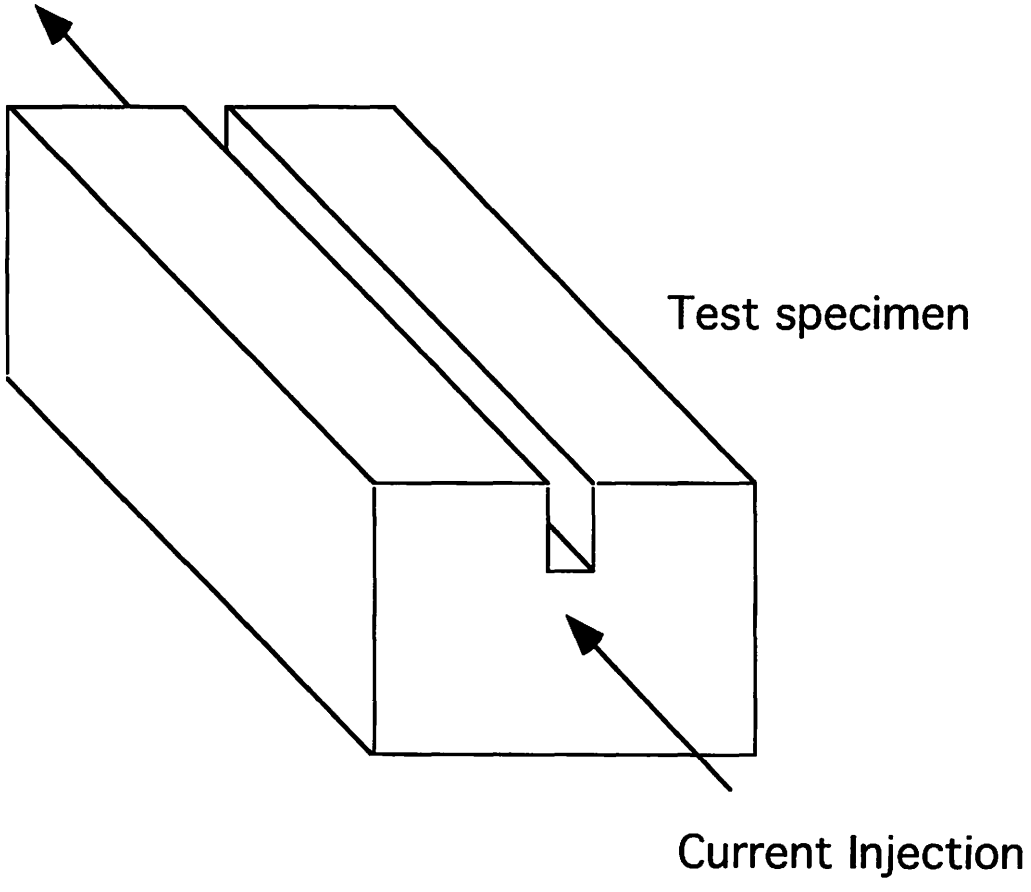

Figure 2.1. Rectangular bar with current injection

defect at the center of its upper face running along its entire length as shown in Figure 2.1.

Closed magnetic lines of flux are set up encircling the current. The orientation of the lines of flux is in the clockwise direction as given by Ampere's law. The intensity of the lines changes from zero at the center of the specimen to a maximum on the surface. In the presence of the defect, the lines of flux on the upper surface get redistributed resulting in an increase of flux density just below the defect. If the current injection is sufficient, the region under the defect gets saturated decreasing its permeability drastically. At this juncture different points of the specimen operate at different points of the magnetization curve. Since the flux lines always follow the path of least reluctance, some flux leaks into the air above the surface. This flux can be detected by using a sensor indicating the presence of the defect [4] [7] [12] [18]. This is shown by Figure 2.2 (a) and (b).

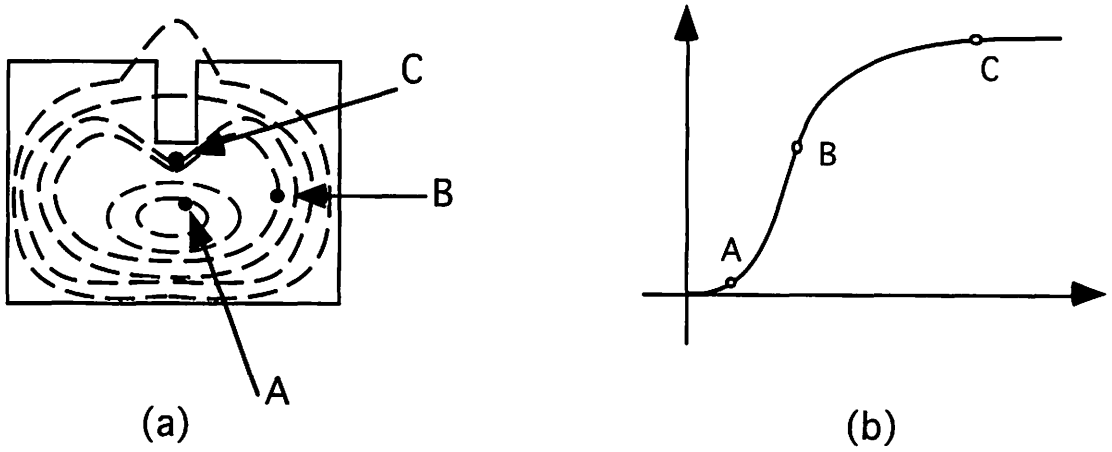

Figure 2.2 (a) The test specimen and (b) its magnetization curve

The sensor can be oriented such that it measures the normal or tangential component of the flux density. Typical plots of the normal and tangential components of the flux density are shown in Figure 2.3 (a) and (b) [2] [9] [11]. Generally, the normal component is measured as the location of its peaks gives an estimate of the size of the defect.

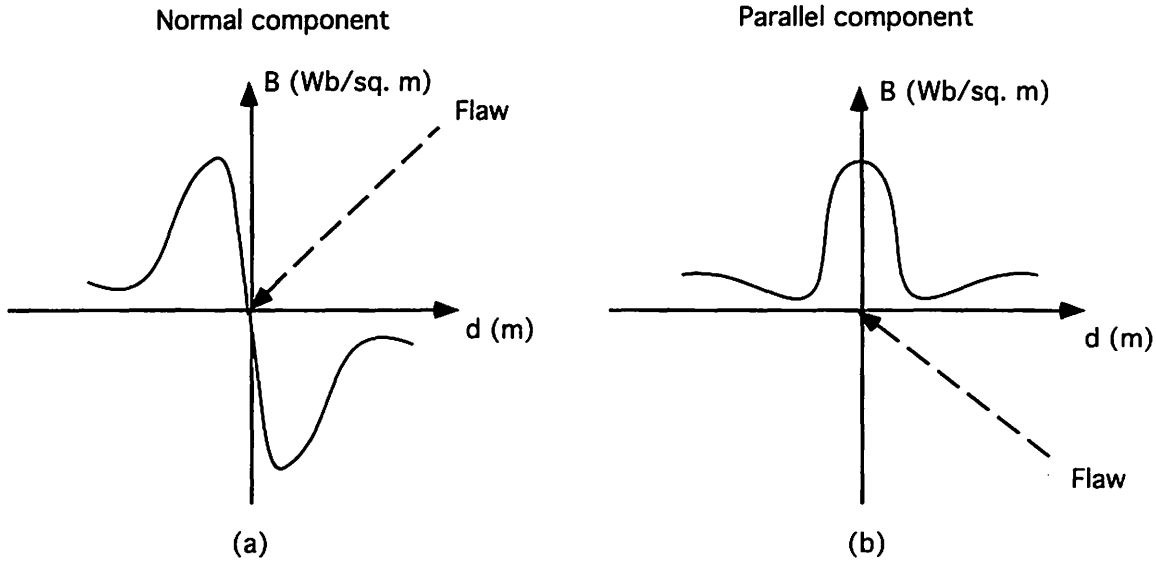

Figure 2.3 (a) The normal and (b) parallel component of flux density

The governing equations for the active MFL method are obtained from variations of Maxwell's equations for the magnetostatic case. They are shown in equations (2.1), (2.2), (2.3) and (2.4) [8].

$$\nabla \times \bar{H} = \bar{J} \tag{2.1}$$

$$\nabla \times \bar{E} = 0 \tag{2.2}$$

$$\nabla \cdot \bar{B} = 0 \tag{2.3}$$

$$\nabla \cdot \bar{D} = \rho \tag{2.4}$$

Also,

$$\bar{B} = \mu \bar{H} \tag{2.5}$$

$$\bar{D} = \varepsilon \bar{E} \tag{2.6}$$

where,

∇ = the vector differential operator,

H = magnetic field intensity (in Ampere per meter),

J = current density (in Ampere per square meter),

E = electric field intensity (in Volt per meter),

D = electric flux density (in Coulomb per square meter),

μ = magnetic permeability (in Henry),

ε = permitivitty (in Farad per meter).

The divergence of the magnetic flux density is zero and hence it can be expressed as the curl of the magnetic vector potential as shown in equation (2.7)

$$\bar{B} = \nabla \times \bar{A} \tag{2.7}$$

where,

A = magnetic vector potential.

Substituting equations (2.5) and (2.7) in equation (2.1),

$$\nabla \times \frac{1}{\mu}(\nabla \times \bar{A}) = \bar{J} \tag{2.8}$$

However, for a homogenous medium, choosing Coulomb's gauge, the following vector identity holds [8].

$$\nabla \times (\nabla \times \bar{A}) = \nabla(\nabla \cdot \bar{A}) - \nabla^2 \bar{A} = -\nabla^2 \bar{A} \tag{2.9}$$

Thus substituting equation (2.9) in equation (2.8), the final governing equation for a homogenous medium can be written as shown in equation (2.10) [18]

$$\frac{1}{\mu}\nabla^2 \bar{A} = -\bar{J} \tag{2.10}$$

Residual MFL method

The fundamental concept behind the residual MFL method is the same as that of the active MFL method except that there is no source of active magnetization. Rather, the magnetic domains of the material orient themselves in such a way that the leakage field is

maintained. However the leakage field signals obtained in this method are significantly lower. From the B/H curve standpoint, the operating points of the specimen relax to a straight line in the second quadrant in order to satisfy Ampere's law [21] [22]. This is demonstrated in Figure 2.4.

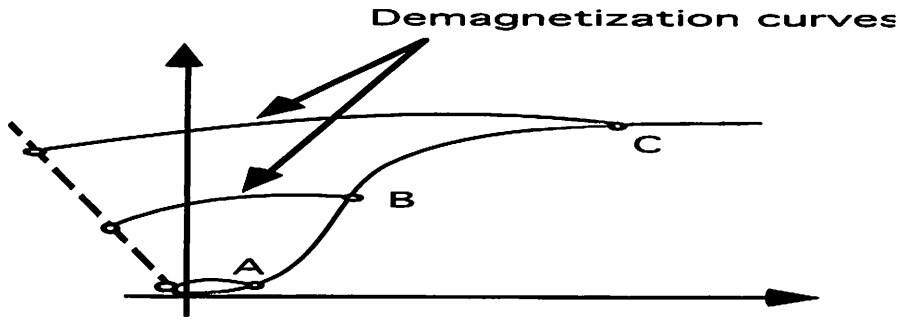

Figure 2.4. The relaxation curves of the operating points

Since the operating points relax to the second quadrant, the remnant magnetization in the material is represented by an equivalent current density 'J_m'. Hence the governing equation (2.10) gets modified as shown in equation (2.11).

$$\nabla \times \frac{1}{\mu}(\nabla \times \bar{A}) = -(\bar{J} + \bar{J}_m) \tag{2.11}$$

along with the interface condition

$$\nu_1 B_{t1} - \nu_2 B_{t2} = j_m \tag{2.12}$$

where,

J = source current density.

J_m = volume current density,

ν_1 = reluctivity of medium 1,

ν_2 = reluctivity of medium 2,

B_{t1} = tangential component of B in medium 1,

B_{t2} = tangential component of B in medium 2,

j_m = surface bound current.

The volume current density is expressed as

$$\bar{J}_m = \nabla \times \bar{H}_0 \tag{2.13}$$

where,

H_0 = magnetic field intensity when B is zero.

The exact solution of the governing equations can be obtained analytically only for simple geometries. In more realistic test situations, complex geometries and difficult boundary conditions have to be dealt with. In such a case analytical methods do not converge easily to the solution. Hence numerical methods such as finite element or finite difference methods are preferred [16] [20] [23]. These methods have been extensively used to model the MFL, eddy current, and other electromagnetic phenomena.

Eddy current NDE methods

In this method of NDE, eddy currents are caused to flow in the test object by electromagnetic induction. A sinusoidal constant amplitude current is impressed on a test coil. This produces a sinusoidal magnetic field which induces a sinusoidal voltage in the test specimen as given by Faraday's law. This voltage causes currents to flow in the test specimen such that their field opposes the very cause that produces them. (given by Lenz's law.) These currents are called eddy currents. In the absence of any resistive losses, the field produced by the eddy currents would exactly be 180 degrees out of phase with the primary field. However, in practice the resistivity of the test specimen is significant. Hence the signal read across the coil terminals is a voltage resulting from a vector combination of the primary and secondary fields. The presence of a discontinuity in the specimen changes the impedance in the path of the eddy currents changing the measured voltage.

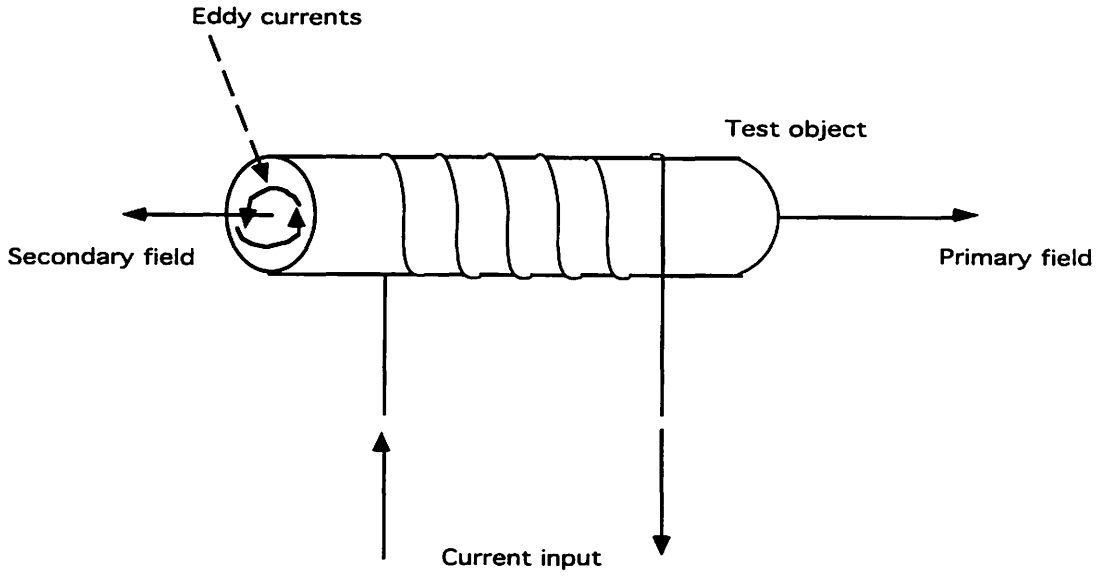

Figure 2.5. The eddy current NDE method

It is important that the input voltage be constant in magnitude and frequency for the duration of the test. This is because the impedance of the test object is a function of both the frequency and the input voltage.

An important consideration in eddy current testing is the choice of frequency. The resistive component of the impedance of the test object results from magnetic hysteresis as well the eddy current phenomena. The hysteresis losses are proportional to the input frequency while the eddy current losses are proportional to the square of the frequency. Thus the greater the frequency of excitation the larger the sensitivity to eddy currents. In practice a frequency of 500 to 500,000 Hz is used for eddy current NDE methods [12].

The equivalent circuit of an eddy current measurement scenario is similar to a transformer with a one turn short circuited secondary coil. This model can explain the change of the measured voltage effectively. However, the parameters in the circuit are themselves difficult to calculate making this approach impractical. The equivalent circuit is shown in Figure 2.6.

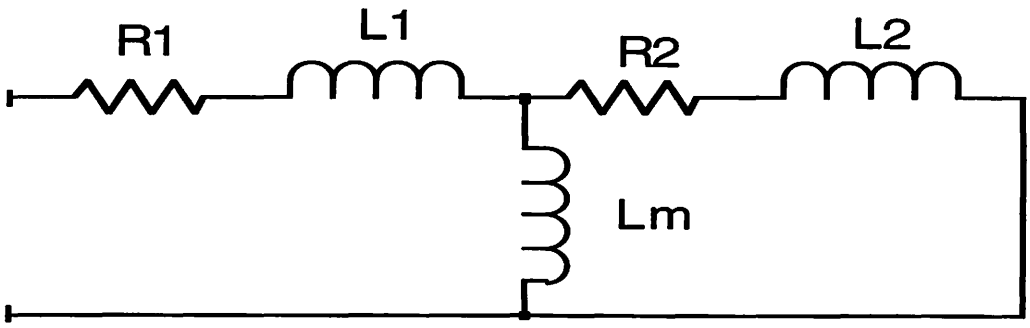

Figure 2.6. The equivalent circuit of the eddy current measurement

In the above circuit,

R_1 = resistance of the primary coil,

R_2 = resistance to the eddy currents,

L_1 = leakage inductance of the primary coil,

L_2 = equivalent leakage inductance,

L_m = inductance to account for the quiescent current.

A phasor diagram can be drawn for the above circuit (as shown in Figure 2.7) to represent the phase of all the relevant currents and voltages with respect to each other. The reference phasor is the flux (φ). The diagram is referred to the primary coil The other symbols used in the phasor diagram are:

N = number of turns of the primary coil,

X_1 = reactance of the primary coil,

X_2 = reactance of the test specimen,

I_m = magnetizing current,

V_1, V_2 = primary and secondary voltages,

I_1, I_2 = primary and secondary currents,

V_{in} = input voltage.

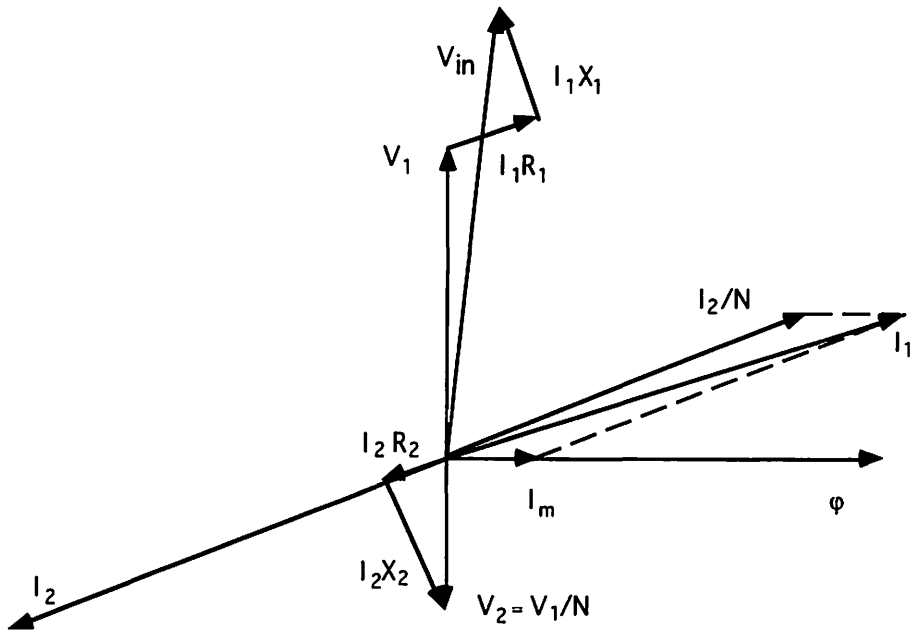

Figure 2.7. The phasor diagram for the eddy current measurement

The eddy current NDE method is used for detecting discontinuities in electrical conductors. It is extremely sensitive to the variation of the magnetic properties of the material. A magnetic saturation technique can be used to reduce this interference to an acceptable level [12].

The governing equations for this method are obtained from variations of Maxwell's equations for time varying low frequency sinusoidal fields. They are displayed in equations (2.14), (2.15), (2.16) and (2.17) [8].

$$\nabla \times \bar{H} = \bar{J} \tag{2.14}$$

$$\nabla \times \bar{E} = -\frac{\partial \bar{B}}{\partial t} \tag{2.15}$$

$$\nabla \cdot \bar{B} = 0 \tag{2.16}$$

$$\nabla \cdot \bar{D} = \rho \tag{2.17}$$

where,

ρ = volume charge density.

Substituting equation (2.7) in equation (2.15)

$$\nabla \times \bar{E} = -\nabla \times \frac{\partial \bar{A}}{\partial t} \tag{2.18}$$

Equation (2.18) can also be expressed as

$$\nabla \times (\bar{E} + \frac{\partial \bar{A}}{\partial t}) = 0 \tag{2.19}$$

Using vector identities, a scalar potential 'Φ' can be defined such that

$$\bar{E} + \frac{\partial \bar{A}}{\partial t} = -\overline{\nabla \phi} \tag{2.20}$$

Also,

$$\bar{J} = \sigma \bar{E} \tag{2.21}$$

where

σ = electric conductivity.

Substituting equation (2.21) in equation (2.20)

$$\bar{J} = -\sigma \frac{\partial \bar{A}}{\partial t} - \sigma \overline{\nabla \phi} \tag{2.22}$$

From equations (2.22) and (2.8), we obtain

$$\nabla \times \frac{1}{\mu}(\nabla \times \bar{A}) = \sigma \frac{\partial \bar{A}}{\partial t} - \bar{J}_s \tag{2.23}$$

where J_s is the source current density representing the second term in equation (2.22). The first term represents the induced eddy current density.

For sinusoidal varying fields the magnetic vector potential 'A' can be expressed as

$$\bar{A} = |A| e^{j\omega t} \tag{2.24}$$

where,

j = square root of -1,

ϖ = the input frequency.

Hence substituting equation (2.24) in equation (2.23) the final governing equation for single frequency eddy current phenomena can be written as

$$\nabla \times \frac{1}{\mu}(\nabla \times \bar{A}) = j\varpi\sigma\bar{A} - J_s \tag{2.25}$$

The magnetic field during eddy current testing decays exponentially with the depth inside the material. Hence eddy current methods of non-destructive testing are generally not very effective in detecting deep subsurface flaws, The amplitude of the magnetic field falls to 1/e times its value at the surface at a depth called the skin depth. For an infinite sheet of current, the value of the skin depth is found to be

$$\delta = \left(\frac{2}{\varpi\mu\sigma}\right)^{1/2} \tag{2.26}$$

where,

δ = skin depth.

This provides an index for the effectiveness of the eddy current phenomenon. It is actually a function of the excitation frequency, permeability and conductivity of the material.

Microwave NDE methods

At very high frequencies, electromagnetic fields can be concentrated into beams and propagated through space. These beams are called microwaves. When such a microwave pulse strikes a conducting surface it is reflected to return as an echo to the site of the original pulse transmitter or to other detectors. This reflection is affected by flaws present in the surface layers of the conducting material. In dielectric materials, microwaves are subjected to rotations and phase shifts, as well as attenuation due to dielectric hysteresis

losses. This response of the microwaves in the presence and the absence of discontinuities is significantly different. This is used to detect discontinuities in the dielectric material.

The choice of microwave frequency and beam size is primarily dependent on the test application and the physical properties of the material under test. Microwave frequencies ranging from 0.3 GHz to over 100 GHz are common. Also typical beam sizes range from a few millimeters to a meter. Two types of sensors are commonly used viz. a reflectometer sensor and a bistatic sensor. The reflectometer sensor has the capability to transmit as well as receive microwaves. It is compact and easier to use. The bistatic sensor has a separate transmitter and a receiver. This mode permits a versatility in the measurements due to the ability to measure a through transmission. Some common sensor arrangements are illustrated in Figure 2.8 [12].

Imaging techniques are commonly applied to measure and display the response of the test specimen to microwaves. This makes it possible to apply a whole range of image processing algorithms and mathematics to process the data The behavior of microwaves is governed by Maxwell's equations for time varying fields.

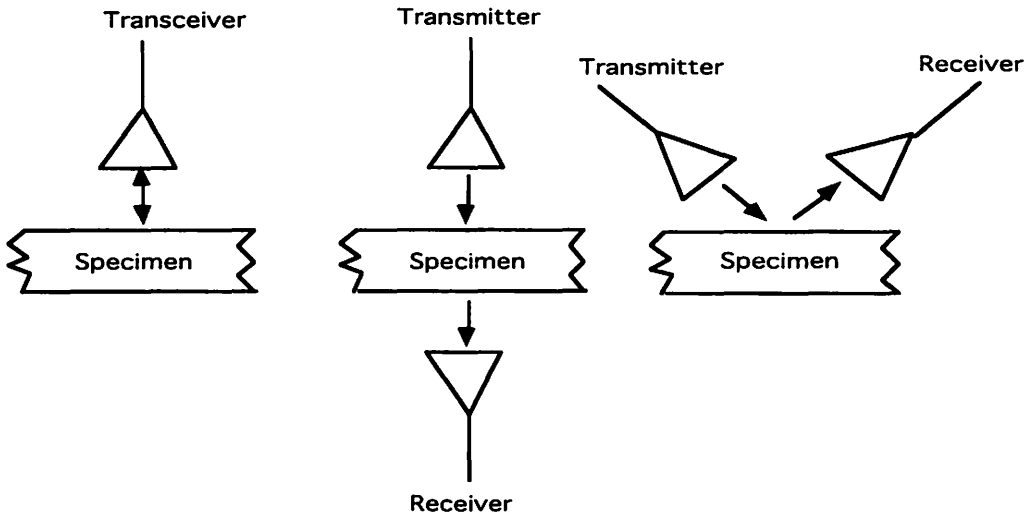

Figure 2.8. Common sensor arrangements for microwave NDE methods.

$$\nabla \times \vec{H} = \vec{J} + \frac{\partial \vec{D}}{\partial t} \tag{2.27}$$

$$\nabla \times \vec{E} = -\frac{\partial \vec{B}}{\partial t} \tag{2.28}$$

$$\nabla \cdot \vec{B} = 0 \tag{2.29}$$

$$\nabla \cdot \vec{D} = \rho \tag{2.30}$$

The advantage of microwaves is their non-contact nature and ability to penetrate deep within the test material. This has made them useful for thickness measurements and detection of embedded flaws. Other uses include moisture gauging.

The rest of this thesis focuses on magnetic particle inspection techniques which are based on the magnetic flux leakage NDE method. A detailed explanation of these techniques is included in the following chapter.

CHAPTER 3. MAGNETIC PARTICLE INSPECTION (MPI) METHOD OF NDE

Fundamentals

The magnetic particle inspection (MPI) method of nondestructive evaluation is a method for detecting surface and subsurface discontinuities in ferromagnetic and paramagnetic specimens. When a specimen is magnetized, the discontinuities lying transverse to the direction of the magnetic field cause a leakage field to be formed above its surface. The leakage field can be detected by a variety of sensors such as Hall elements, induction coils etc. In the MPI method the presence of the leakage field is detected by the use of finely divided ferromagnetic particles which are collected and held by the leakage field [6]. There are many factors which influence the effectiveness of this method. Some are [4]:

1. Direction and strength of the magnetic field.
2. Method of magnetization.
3. Size, shape and direction of the discontinuity.
4. Properties of the magnetic particles.
5. Magnetic characteristics of the specimen under test.

The MPI method is the most sensitive means available to locate very fine and very shallow cracks in ferromagnetic materials. It is effective for surface breaking discontinuities but also works for discontinuities lying slightly below the surface. The indications become weaker as the depth below the surface increases. Soft steels having a high permeability have shown better results with this method as compared to hardened steels and alloys with a lower permeability. Gray or malleable iron castings are also ideal specimens for this method [19].

The method has numerous advantages. Some are [4]:

1. It is rapid and simple.
2. There is no limitation on the size or shape of the test specimen.

3. No elaborate pre-cleaning of the test specimen is required.

4. It is inexpensive.

5. There is no additional equipment required for the motion of sensors as in other methods.

However this method also has some limitations as outlined below:

1. It works only for ferromagnetic and paramagnetic materials.

2. It is ineffective for locating discontinuities far below the surface of the specimen.

3. Demagnetization of the test specimen is required following the test.

4. High magnetic fields are sometimes required to produce adequate results.

The MPI method compares well with other popular NDE methods such as Radiographic, Ultrasonic and Eddy Current methods. Radiographic and Ultrasonic methods are better than the MPI method for the detection of flaws embedded deep inside the specimen. However they are time consuming and expensive. Shallow cracks cannot be easily detected by the Ultrasonic method. Also, the shape of the specimen is much more critical in these methods. The Eddy current method is subject to limitations similar to the Ultrasonic method. A critical size of the flaw is required to cause an imbalance in the impedance bridge and secure readable indications. Eddy currents in conjunction with magnetic saturating bias fields are sometimes better for the detection of subsurface discontinuities but they cannot penetrate significantly beyond the skin depth. Moreover, eddy current methods are greatly influenced by the shape of the test specimen.

Due to the inherent superiority of the MPI method in finding shallow cracks in ferromagnetic specimens, it is the best method for the detection of fatigue cracks. Fatigue cracks occur in parts which are highly stressed. Starting at the surface and propagating inwards, they cause a breakdown of the specimen. However the MPI method can detect these cracks early and thus prevent more catastrophic failures. The MPI method involves three essential steps viz. magnetization of the test specimen, application of ferromagnetic particles and the inspection of the surface for indications of defects. These are described in

the following sections.

In the testing of steel billets, magnetic particle sensors are used differently than in the normal MPI method. In this case, it is often necessary to detect surface cracks and to distinguish between surface and subsurface flaws. The former can be removed by grinding while the latter are worked into the final product in the form of laminations. Magnetic tapes have been developed for such applications. The magnetic tape is made from finely divided ferrite particles embedded in wear resistant neoprene. These particles become magnetized by flaw MFL fields. Different localized regions are magnetized with different magnitudes as the tape passes over the surface of the specimen. This magnetization can be interpreted to indicate the location and the extent of the flaw. Magnetization of the ferrite particles is low because of the large demagnetization factors associated with finely ground materials. One major advantage of the magnetic tapes is that they are reusable. The signals on the tapes can be erased and they can be used for subsequent testing. This method has also been used widely for inspection of tubing and flat plates.

Magnetization methods

A variety of methods is used for magnetizing a test specimen. Some of the common methods are outlined below [19].

Earth's magnetic field

The Earth is in effect a huge permanent magnet with a north magnetic pole just north of Prince of Wales island in Northern Canada and a south pole just off the coast of the Antarctic Continent at Commonwealth Bay. The flux lines of the Earth's field circle the globe in a generally north - south direction and concentrate at the poles. The earth's field is quite weak compared to the strength of the fields used in the MPI method. However it is worth a mention since long bars of iron can be magnetized to an appreciable degree by placing them

for a long time in the in the north - south direction. Magnetization can be hastened by striking the bars with a hammer to vibrate them.

Magnetization with permanent magnets

Permanent magnets can be used to magnetize parts for MPI testing. However, permanent magnets are capable of setting up only longitudinal fields. Poles are present on the specimens because of contact with the poles of the permanent magnets used. This may result in the adherence of the magnetic particles to the poles. The field strengths obtained by this method are much lower than required. Sometimes the control of the permanent magnet field is possible only in limited areas. This can be seen in the case of a bar magnet attempting to magnetize a thin plate. The flux of this field leaves the plate surface at some distance from the point of contact to return to the pole at the opposite end of the magnet as shown in Figure 3.1.

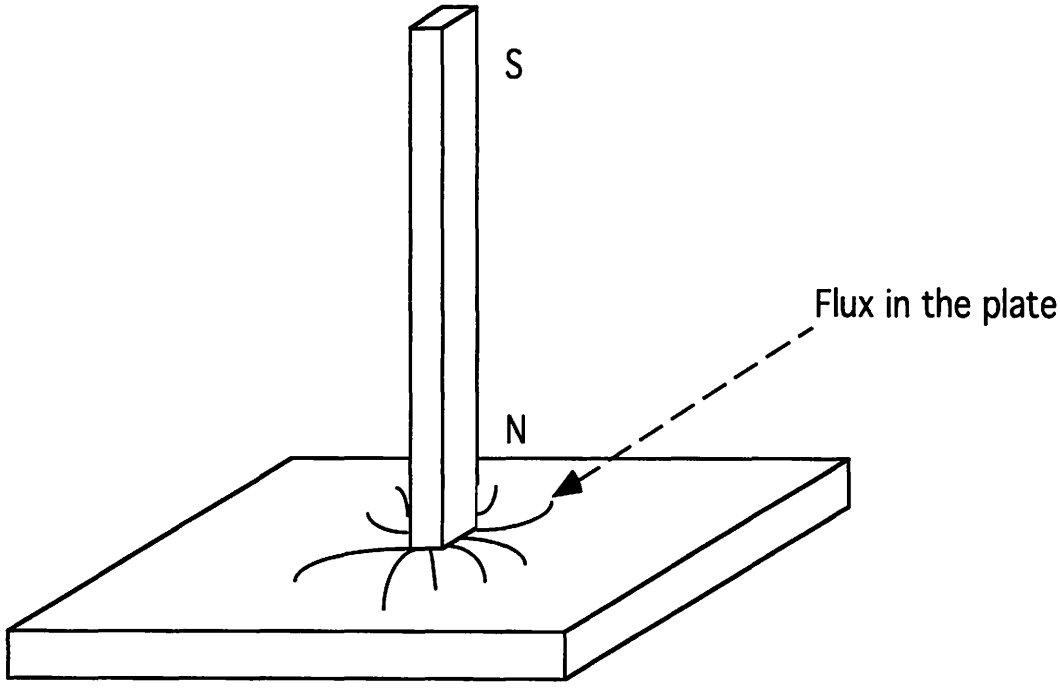

Figure 3.1. Magnetization of a plate using a bar magnet [19]

Other drawbacks of this method include the inability to vary the strength of the magnetic field, the difficulty in separating the magnet from the part especially if the field is strong and the inability to produce defect indications for large size specimens.

Electric currents for magnetization

This technique of magnetization is extremely popular. Longitudinal and circular fields can be set up easily. The strength of the field can be varied by changing the magnitude of the current. Also the nature of the current (e.g. alternating or dc) can realize several nature of fields. The directional properties of the field depend on the shape of the current carrying conductor. If the current passes through a single straight wire the magnetic lines of force are circular in the plane perpendicular to the direction of current. However if the current passes through several turns of wire wound on a rod shaped material the field is along the axis of the rod as illustrated in Figure 3.2.

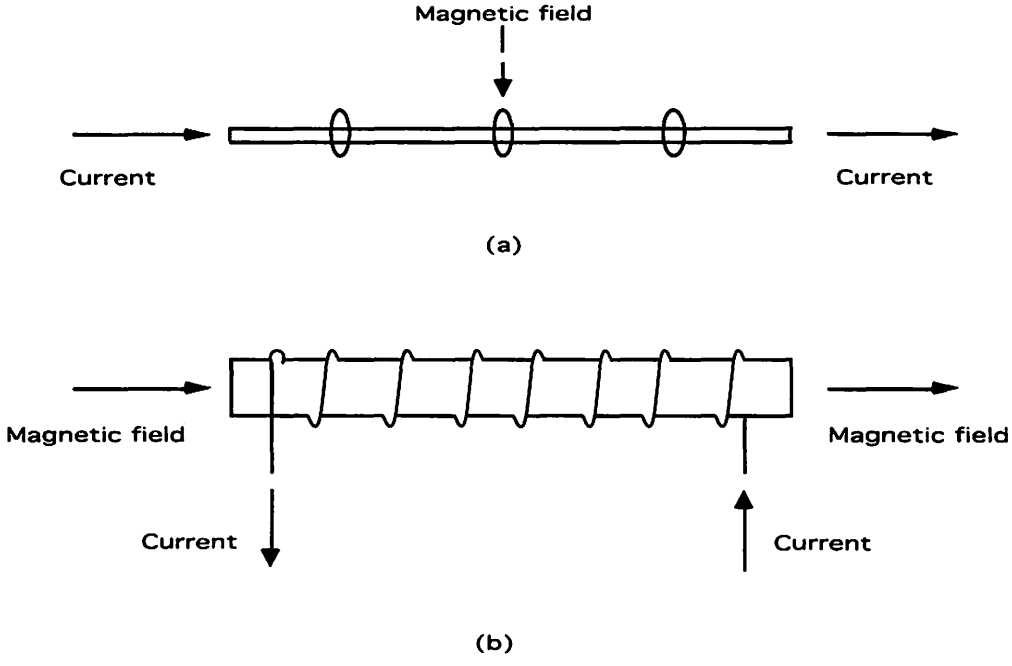

Figure 3.2 (a) Circular and (b) longitudinal direction of the magnetic field

Longitudinal magnetization is used when the orientations of the defects are perpendicular to the long axis of the specimen. But due to the polarity associated with longitudinal magnetization, external leakage fields interfere with background patterns. This is not the case with circular magnetization. Hence circular magnetization is generally preferred. A solid ferromagnetic specimen is magnetized circumferentially by passing a current through it along its long axis. In this case the internal magnetic flux density is zero along the central axis and increases to a maximum on the surface. In the air surrounding the specimen the flux density rapidly decays to zero because of the low permeability of air. If the ferromagnetic specimen is hollow (e.g. a tube) then the best strategy of magnetization is to pass current through a central conductor threaded inside the tube. In such a case however, the flux density will be maximum on the inner surface of the tube and somewhat less on the outer surface. An important consideration while injecting the current is the type of contacts. It is important to ensure that the contact pressure is adequate and the contact area is clean. In the absence of these precautions arcing could occur due to the increase in current density over distributed regions of the contact. Also another important precaution is while breaking the circuit. The inductance associated with the ferromagnetic specimen can give a tremendous "back" voltage if the current is broken very rapidly. Hence great care must be taken to reduce the current in steps. In case of ac magnetization the circuit is broken when the current waveform crosses its natural zero.

The nature of the field depends on the nature of the current i.e. dc, alternating or transient. The main consideration of choice between ac and dc is the skin effect. The tremendous inductance associated with a ferromagnetic material causes a pronounced skin effect at commercial ac frequencies of 60 Hz. Therefore for embedded flaws the magnetization of choice is dc. Common sources of dc include dc generators, ac rectifiers and storage batteries, etc. Transient currents take advantage of the hysteresis phenomenon to get higher magnetization for the same current. When a high transient current is applied

prior to the steady current the operating point of the ferromagnetic material settles to the higher value of flux density. Common sources of transient currents are highly charged condensers, thyristorized circuits, etc.

Magnetic particles and particle application

There are two types of MPI tests distinguished by the type of magnetic particles used.

Dry method

Particles used in the dry method are finely divided iron particles coated with fluorescent pigments. These particles have a low coercive force and low retentivity. If the particles have a high retentivity then they adhere to each other and cannot be applied properly. High permeability and low coercivity are necessary for greater sensitivity to leakage fields. The pigments emit visible light when excited by ultraviolet radiation. Although these pigments degrade the magnetic properties the visibility is increased and hence it is necessary to compromise the need for sensitivity and high visibility. Other factors influencing the sensitivity are the physical properties of the particles including the size and shape. The particles used commercially are no larger than 150 μm in any dimension [19]. Commercial particles used are usually a mix of circular and elongated particles. The elongated particles have greater sensitivity to the field while the circular particles prevent the clustering of elongated particles having a strong directional orientation. Also circular particles give the mixture larger mobility.

Dry particles are applied in a gentle stream with a low velocity. Manual or mechanized powder applicators can be used effectively to this end. It is recommended that dry particles be used only once. This is because the physical properties of the dry powder deteriorate with each use. Also, the pigments on their surface wear out resulting in less visibility. The

dry powders are usually stored in a moisture free environment at room temperature. The dry method usually works better than the wet method for larger and longer flaws.

Wet method

Particles used in the wet method are generally finely divided iron, iron oxide, ferrite, nickel, and nickel alloys. They are coated with fluorescent pigments similar to the dry method and a bonding resin. The size of particles used in the wet method is finer than in the dry method. Commercial particles are no greater than 15 μm in any dimension [19]. They are generally compact for low retentivity. The clustering of the magnetic particles in the wet method is more significant than in the dry method.

The wet particles are suspended in a bath of oil or water. The bath is under frequent agitation to prevent clustering of the particles. Oil baths are generally preferred because they are non-corrosive and pose no electrical hazard. However these are costlier to maintain than the water baths. Also they reduce mobility of the particles due to high viscosity. In the wet method, the suspension of particles in an oil bath is applied to the test specimen before the magnetic field is applied. Once the application process is complete, the test specimen can be magnetized in different orientations to obtain reliable indications of the flaw. The wet particles are stored at moderate temperatures in a contaminant free environment. In general the wet method is shown to produce better results than the dry method for small and shallow flaws.

Recording of MPI data

Until the early 1950s, the human eye was used to detect defect indications. However, more recently, electro-optical devices are used to detect indications of a discontinuity and computers are used to interpret the data. Automatic scanners usually comprise of the following components [19]:

1. A source of ultraviolet radiation

2. A photodetector sensitive to visible light.

3. An imaging apparatus such as a television or a flying spot system.

4. Signal processing equipment.

These components are integral to two basic types of scanning systems described below. Both the systems have been used widely in the industry. Each has some advantages and disadvantages.

Television scanners

A television scanner first illuminates the test object with filtered ultraviolet light. The camera is used as a detector of visible indications. It is equipped with a image intensifier and a filter to remove superfluous ultraviolet light. The output video signal is processed through a computer designed to distinguish noise from discontinuities. In case a discontinuity is detected the computer sorts the test object to the reject bin. Pattern recognition and classification algorithms are employed for this purpose. The principal advantage of these systems is that they are inexpensive and simple to configure. All accessories are readily available.

Flying spot scanners

The flying spot scanners use a narrow and intense beam of ultraviolet light to illuminate the test object. The source of the beam is usually a laser. The scanning occurs as the beam passes over the test object and illuminates a small area at one time. The detection is thus in the form of pulses rather than continuous as in the television scanner. Signal processing is used to distinguish discontinuities from background noise. These systems are more expensive. However, they are capable of producing large intensities of fluorescence and thus are more effective than the television scanners. However the configuration of these systems is complex.

Interpretation of MPI data

Recognition of significant test indications and distinguishing them from the background indications are two complex problems for computerized MPI testing. The output from a scanner is typically analog and needs to be digitized before it can be processed by a computer. A typical block diagram of this conversion is shown in Figure 3.3.

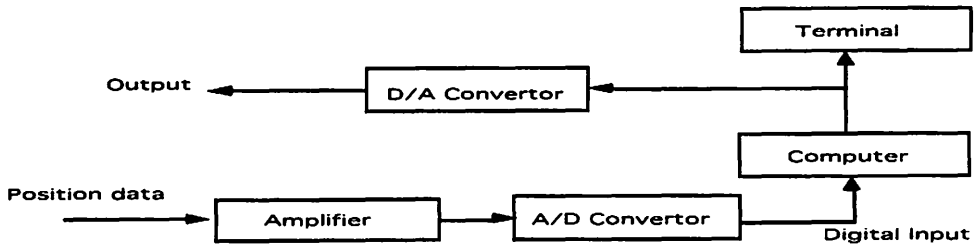

Figure 3.3. Conversion of analog test signals into digital input data

The input to a computer is typically in the form of a scanner memory matrix. This matrix has ones and zeros due to thresholding. An example of this matrix is shown in Figure 3.4. In practice however, the matrix can be much larger than this depending on the resolution of the scanner.

0	0	0	0	1	0	0	1	0	1	0	0
0	0	0	0	0	0	0	0	0	0	0	0
0	0	0	0	0	0	0	0	0	1	1	1
0	0	0	0	1	1	1	1	1	0	0	0
1	1	1	1	0	0	0	0	0	0	0	0
0	0	0	0	0	0	0	0	0	0	0	0
0		0	0	1	0	0	0	0	0	0	0
0	0	0	0	0	0	0	1	0	0	1	0

Figure 3.4. Scanner memory matrix [19]

This matrix can be treated as a binary image and further processing can be carried out using pattern recognition and image processing algorithms. Some commonly used algorithms are briefly described.

Adjacent cell linking [19]

The adjacent cell linking algorithm uses the heuristic that the longer the "1" chain, the better the probability that it is caused by a flaw. Initially the scanner data is stored in memory with addressing referenced to the position of discontinuity in the test object. Horizontal discontinuities can be detected by the following algorithm. Assuming a matrix X of size m x n and a preset threshold length N for detection of the flaw, for every row of the matrix repeat the following steps:

1. Start
2. position = 1
3. True_flaw = 0
4. Check the value of X(position)
5. If X(position) = 1 then

   position = position + 1.

   True_flaw = True_flaw + 1

   Goto step 4.
6. If True_flaw > N then a flaw is present
7. position = position + 1
8. If position > size of the matrix stop else goto step 3.

Variations of this algorithm can be used for detecting vertical and angular discontinuities. For vertical discontinuities, the position index to be incremented is altered. However for angular discontinuities the Euclidean distance is incremented rather than the position index itself.

SRI algorithms [19]

A popular set of pattern recognition algorithms have been developed by the Standard Research Institute which can be used for the interpretation of MPI data. These algorithms consist of a series of procedures that control about fifty different features extracted from a binary image. The features include the size of the blank area, the centroids of illuminated areas, the size of illuminated areas etc. These features are then compared with features of bench mark defects already available in the database. The chief drawback of the SRI algorithms is the large computation time due to large sizes of the matrices. Another requirement is the availability of an extensive database for interpretation and classification.

Neighborhood processing [19]

Neighborhood processing is also known as cellular automata or morphological image processing. In this technique, each pixel of the image is converted in a particular way that primarily depends on the state of the neighboring pixel and a transition rule. There are four key stages of processing. First, the pixel word acquires gray levels in the least significant bit and other information in more significant bits. Second, a series of successive transformations occur in a carefully determined sequence. Third, the irrelevant data is eliminated and the important information is stored in the most significant bit. Finally, the image is scanned and specific features are studied by examining certain bits. The advantage of neighborhood processing is that it removes background noise very effectively. It is then easy to use spatial gating of a video image system to trigger alarms or other warning devices.

There are many other sophisticated image processing algorithms which can be used effectively to characterize the MPI image. However, the application of these algorithms to the field of magnetic particle inspection has been extremely limited.

CHAPTER 4. THE MPI SIMULATION MODEL

Introduction

This chapter presents a mathematical model for simulating the MPI testing process (the wet method). The goal of this model is to recreate the dynamics of the magnetic particles before they reach an equilibrium around the flaw. In general, the leakage field exerts a large motile force on the particles compared to their mass and flaw indications are typically formed within seconds. The human eye cannot observe the motion of the particles under normal circumstances. However the model has the capability to recreate their motion at a speed that is perceivable by the human eye. The approach can predict the time to equilibrium of the magnetic particles and provide useful data for the design of the imaging system. The model also provides mathematical parameters which can be used to optimize experimental conditions and characterize the MPI data [1].

The model consists of three components viz. a finite element model for the prediction of the leakage fields, a statistical model for the initial distribution of the magnetic particles and a force model for the calculation of the particle dynamics. A schematic of these sub-tasks is shown in the Figure 4.1.

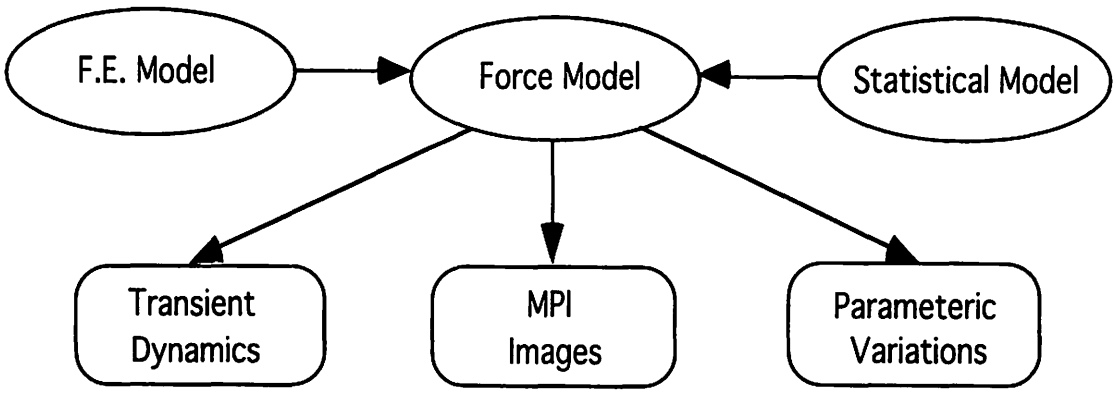

Figure 4.1. Schematic of the MPI simulation model

Statistical model for particle distribution

The particles are sprayed on the surface of the specimen by an automated system or by an operator. It is assumed that the specimen is initially unmagnetized. The ferromagnetic domains of the specimen are randomly oriented such that the net magnetic moment is zero. There is no magnetic force to influence the distribution of particles. Hence, the particles are assumed to be uniformly distributed initially.

The total number of particles sprayed depends on the size of the specimen and the intensity desired for the imaging system. In the model, this quantity is specified by the user. It is further assumed that no magnetization is applied immediately after the particles are sprayed. They are allowed to come to a state of rest to justify their truly random distribution. The random variable is the position of the particle 'p' and its probability density function is given by equation (4.1) [3].

$$p = \frac{1}{A_s} \tag{4.1}$$

where,

A_s = the surface area of the specimen.

The particles themselves are ferromagnetic in nature. In the model a tri-state approximation is made regarding their initial magnetization. It is assumed that the magnetic particles are either unmagnetized or operate at positive or negative saturation. This tri-state assignment is gaussian in nature.

The particle sizes are in the order of microns and the number of particles is generally in the order of 10^6. Thus keeping track of every particle is computationally very expensive. To solve this problem, the surface area of the specimen is discretized by a mesh. The density of the mesh is a function of the computation time and resolution of the image. The denser the mesh greater the resolution, accuracy and computation time. (In this work the same mesh used for finite element analysis of the leakage fields is used as explained in the next section.)

After simulating the initial distribution, the particles belonging to the same mesh element are treated as a cluster. The cluster is assumed to behave as a single entity having a mass given by the summation of the masses of the individual particles and a net magnetic moment which is the vector combination of the individual moments. Assuming 'n' particles in a single mesh element, the mass and the magnetic moment of the cluster of particles in the element can be expressed as

$$m_c = \sum_{i=1}^{n} m_i \tag{4.2}$$

$$\bar{M}_c = \sum_{i=1}^{n} \bar{M}_i \tag{4.3}$$

where,

m_c = mass of the cluster,

M_c = net magnetic moment of the cluster,

$m_1, .. , m_n$ = masses of the individual particles,

$M_1, .. , M_n$ = magnetic moments of the individual particles.

This grouping the particles into clusters results in at most be as many clusters as the number of elements in the mesh. This reduces the computational complexity tremendously at a minimal loss of accuracy. The loss of accuracy is primarily because the interaction between the clusters is ignored.

The physical problem is then mapped to an image matrix which is of the same size as the mesh. Each element of the matrix is a 2 - tupple $\{ m_c, M_c\}_i$ representing the mass and magnetic moment of the cluster located in the corresponding mesh element. For simplicity, this matrix is decoupled to form two matrices, one representing the mass and the other representing the magnetic moment. The complete description of the physical problem is encoded in these two matrices as expressed by the following equations.

$$MPI\_\ image\_matrix = [(m_{q_j}, \bar{M}_{q_j})]_{\substack{i=1..a \\ j=1..b}} \tag{4.4}$$

The decoupled matrices are

$$\text{Mass\_matrix} = [m_{c_{ij}}]_{\substack{i=1.a \\ j=1.b}} \tag{4.5}$$

$$\text{Moment\_matrix} = [\bar{M}_{q_j}]_{\substack{i=1.a \\ j=1.b}} \tag{4.6}$$

where the size of the mesh is "a x b".

Finite element modeling of the leakage fields

Once the particles come to a state of rest, the specimen is magnetized. The magnetization is accomplished using an electromagnet or current injection. As described earlier, the presence of a flaw in the specimen results in generation of magnetic flux leakage fields. These can be measured experimentally or simulated numerically on the computer using theoretical models. In this study, the magnetostatic flux leakage phenomenon is modeled using finite element analysis. This model assumes a longitudinal magnetization with no current sources in the region of interest. This makes it possible to model the flux distribution by solving an energy functional based on the scalar magnetic potential [25] which in turn reduces the computational complexity associated with three dimensional finite element modeling.

As mentioned earlier, the solution of the governing equation for predicting the leakage fields can be achieved using analytical methods only for simple geometries. Finite element modeling is used most effectively for complex geometries. This method is based on the principles of variational calculus [13]. The governing equation is expressed in an integral form using an energy functional. The energy functional, which represents the energy of the system, is then minimized resulting in the solution to the governing equation [11] [15] [16]. The magnetic field intensity 'H' can be expressed in terms of the scalar magnetic potential 'u' as

$$\bar{H} = -\overline{\nabla u} \tag{4.7}$$

where,

∇ = the vector differential operator.

Also,

$$\vec{B} = \mu\vec{H} \tag{4.8}$$

$$\nabla \cdot \vec{B} = 0 \tag{4.9}$$

where,

B = magnetic flux density,

μ = magnetic permeability.

Therefore, substituting equations (4.7), (4.8) in equation (4.9) we get the Laplace equation,

$$\nabla^2 u = 0 \tag{4.10}$$

This can be expressed in the Cartesian co-ordinates as

$$\frac{\partial^2 u}{\partial x^2} + \frac{\partial^2 u}{\partial y^2} + \frac{\partial^2 u}{\partial z^2} = 0 \tag{4.11}$$

and the corresponding energy functional 'F' can be expressed in the Cartesian co-ordinates as

$$F = \iiint_{\Omega} [(\frac{\partial u}{\partial x})^2 + (\frac{\partial u}{\partial y})^2 + (\frac{\partial u}{\partial z})^2] dv \tag{4.12}$$

where,

dv = a differential volume element,

Ω = the volume under consideration.

Once the energy functional is defined, the finite element formulation consists of the following steps [18].

1. The region of interest is discretized with a suitable three dimensional mesh consisting of a number of elements connected at common nodal points. (A two dimensional projection of this mesh is itself used in the statistical model for generating the MPI image matrix).

2. The nodes and the elements of the different materials in the regions are identified and numbered.

3. An interpolating function, which approximates the continuous field over each element in terms of its nodal point values is defined such that the field is continuous across the element boundaries. This function could be linear or non-linear depending on the variations of the field in the geometry.

4. The energy functional is minimized with respect to the unknown nodal point values resulting in a matrix equation.

5. The solution of the matrix equation yields the nodal values of 'u'.

6. These values can then be used to calculate the values of the magnetic flux density and the magnetic field intensity at each nodal point in the geometry.

The non-linear nature of the MFL problem necessitates an iterative computation of the algorithm stated above. This makes the finite element model computationally intensive. To reduce the computational complexity an equivalent linear model (ELM) developed by Zhang et al. [24] has been used in this study. This uses three constant permeability regions to approximate the non-linear behavior of the test specimen. The three regions are displayed in Figure 4.2.

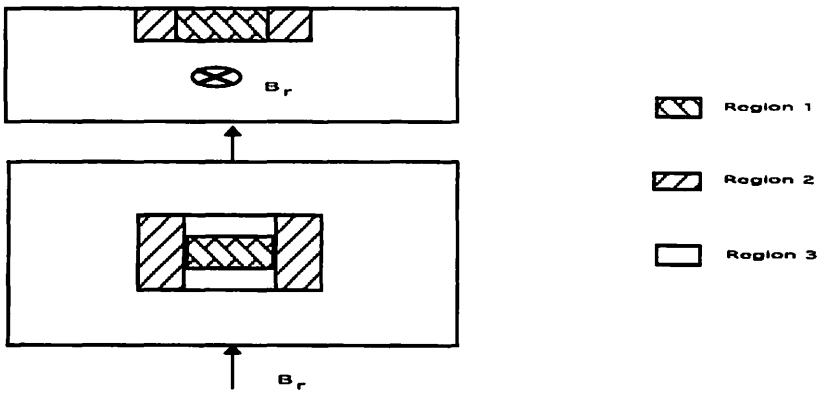

Figure 4.2. The three regions of the ELM

The non-linear nature of the MFL phenomena is understood form its governing equation (Equation (2.10)). Here the value of the permeability 'μ' depends on the vector magnetic potential 'A'. Hence the solution of the governing equation has to be iterative [21]. For convergence, an average MFL calculation involves about 50 - 100 iterations which take about two to three hours on a DEC-3000 workstation.

The partitioning of the specimen into three regions is based on the fact that different regions of the specimen operate at different points on the B-H curve. Regions close to the flaw and perpendicular to the applied field direction tend to operate close to saturation, while the regions close to the flaw but along the field direction operate at low magnetization levels. Hence a single permeability approximation results in an unacceptable loss of accuracy. The dimensions of the three regions are obtained using semi-empirical relations as displayed by equation (4.13).

$$V_r \ \alpha \ V_f \cdot B_r \tag{4.13}$$

where,

V_r = volume of any region (region 1, region 2 or region 3),

V_f = volume of the flaw,

B_r = boundary condition in terms of the flux density.

The permeabilities of the three regions are determined to be

$$\mu_h = 400 \cdot \mu_0 \tag{4.14}$$

$$\mu_s = \frac{175 \cdot \mu_0}{B_r^{\,3}} \tag{4.15}$$

$$\mu_n = \mu \ (B = B_r) \tag{4.16}$$

where,

μ_h, μ_s, μ_n, = permeabilities of regions 1, 2 and 3 respectively.

The performance of the ELM for narrow rectangular flaws is shown by comparing the results with those obtained from the non-linear model.

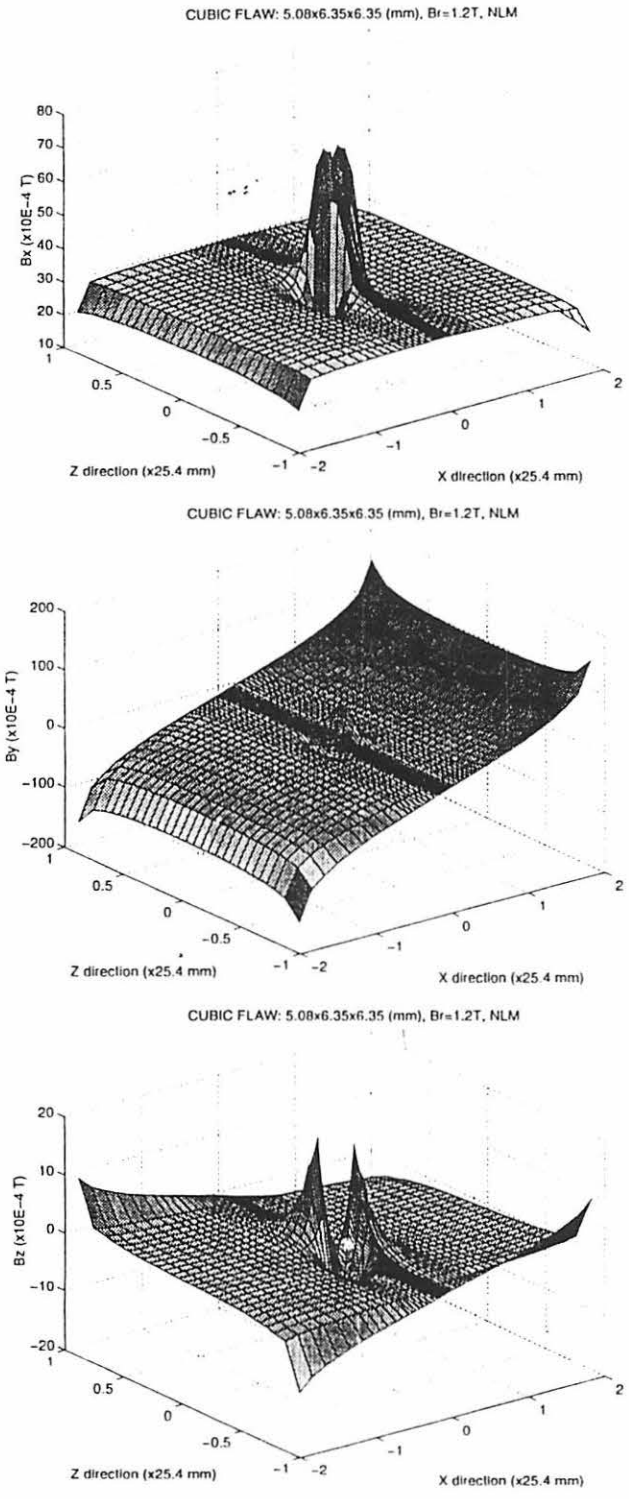

Figure 4.3. The leakage field components using the non-linear model [24]

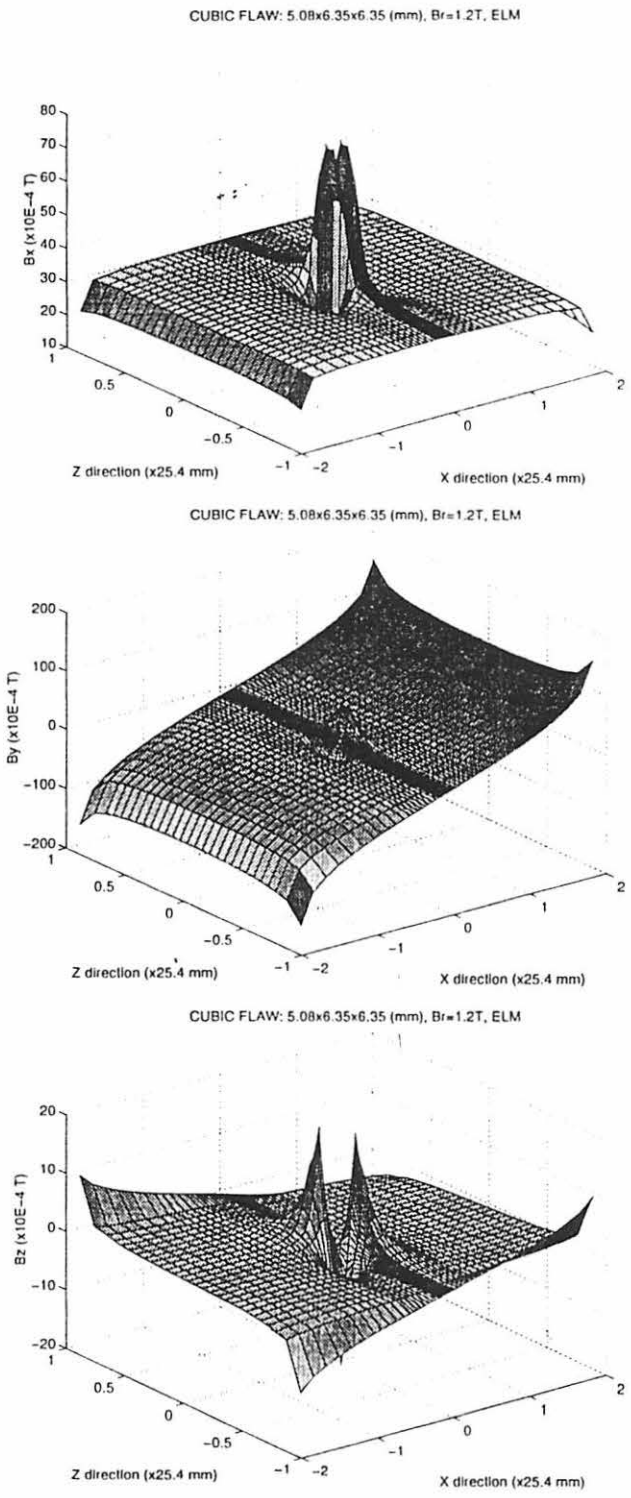

Figure 4.4. The leakage field components using the ELM [24]

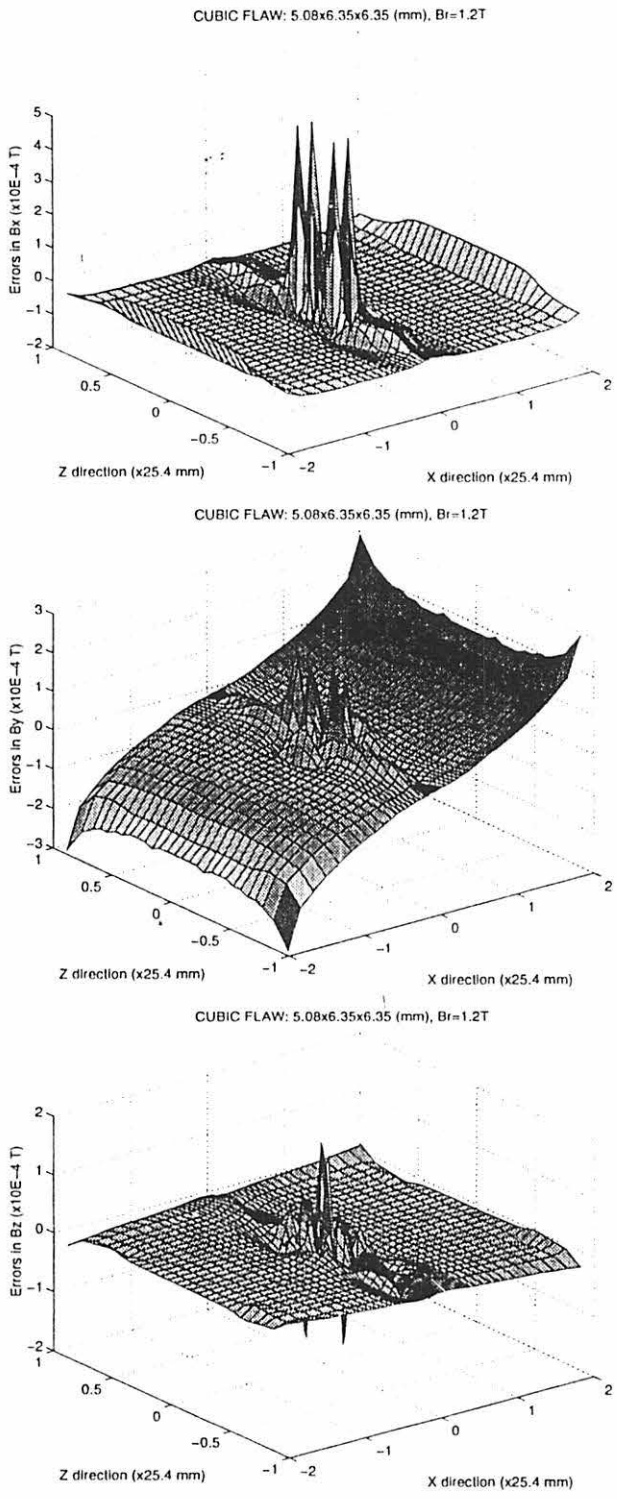

Figure 4.5. Error introduced by using the ELM [24]

Force model for the magnetic particles

The motion of the magnetic particle clusters is influenced by several forces such as the magnetic force due to the leakage fields, the viscous force due to the oil medium, the gravitational force, the interparticle forces, the friction force etc. The extent of their influence on an MPI image however varies considerably. The modeling of the force becomes extremely complicated at a minimal gain of accuracy if all forces are taken into account [7]. In order to simplify the model the following assumptions are made.

1. The test specimen is initially unmagnetized. Hence any magnetic forces due to residual fields are neglected.

2. The effect of inertial, interparticle and viscous forces is neglected because these forces are directly proportional to the mass of the particle clusters which is extremely small.

3. The leakage magnetic field has two effects on the magnetic particle clusters. The magnetic clusters experience an rotational torque, which tends to align their magnetic field to the leakage field, and a translational force which accelerates them towards the flaw. These two effects occur in parallel. However for modeling simplicity it is assumed that these two forces act sequentially on the particle clusters. Further, the time constant of the rotation process is extremely small compared to the time constant for the translational process. This is because the rotational time constant depends only on the strengths of the fields whereas the translational time constant is a function of the specimen dimensions which are large compared to the dimensions of a particle cluster. Hence the rotational process is assumed to be completed instantaneously.

4. The particle cluster is treated as a magnetic dipole aligned with the leakage field at all times.

The mathematical formulation for the force on the particle clusters is described as follows [10]:

For a single magnetic pole of strength 'p' (Ampere-meter) the translational force in a magnetic

field 'H' (Ampere per meter) is given by

$$\bar{F}_t = \mu_0 p\bar{H} \quad \text{(Newton)} \tag{4.17}$$

where,

μ_0 = permeability of free space (in Henry per meter.)

F_t = translational force

Therefore for a magnetic dipole with a separation 'd' (meter) the net force can be expressed as

$$\bar{F}_t = \mu_0 p\bar{H}_1 + \mu_0(-p)\bar{H}_2 \quad \text{(Newton)} \tag{4.18}$$

where,

H_1, H_2 = the magnetic field intensities (in Ampere per meter) at the locations of the two individual poles.

The magnetic moment 'm' of a dipole is given by equation (4.19).

$$m = p \cdot d \quad \text{(Ampere-sq. meter)} \tag{4.19}$$

Substituting equation (4.19) in equation (4.18) the translational force on the dipole can be expressed as shown in equation (4.20).

$$\bar{F}_t = \mu_0 m \frac{(\bar{H}_1 - \bar{H}_2)}{d} \quad \text{(Newton)} \tag{4.20}$$

However in the case of the magnetic particle clusters the distance between the poles is extremely small. Hence equation (4.20) can be approximated as

$$\bar{F}_t = \mu_0 m \frac{\partial \bar{H}}{\partial d} \quad \text{(Newton)} \tag{4.21}$$

Equation (4.21) represents the final model for the force on the magnetic particle clusters located on the surface of the test specimen. It must be understood that 'H' is the magnetic field intensity at the centroid of the cluster. It is assumed that the centroid of the cluster is the center of the mesh element containing the cluster.

The displacements of the particle clusters can be calculated once the forces on them

are known, using Newton's laws of motion. Since the surface of the specimen is mapped onto an MPI image matrix the particles are assumed to move only along the grid composed of the centroids of the mesh elements. Thus any cluster has eight possible directions of motion as illustrated in Figure 4.6.

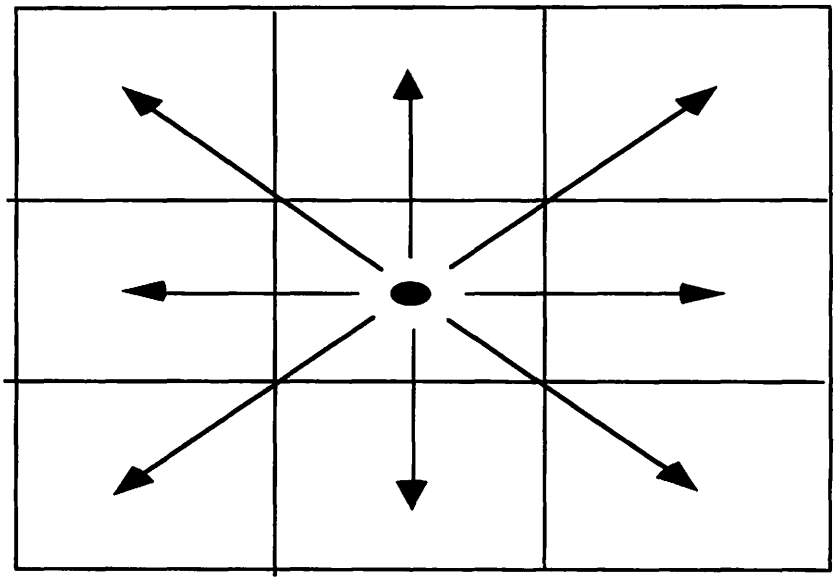

Figure 4.6. Quantized directions of motion of a particle cluster

The equations for the displacement are

$$\bar{a} = \frac{\bar{F}_t}{m_c} \text{ (meters per sq. second)} \tag{4.22}$$

where,

a = acceleration of the magnetic particle clusters.

$$\bar{s} = \bar{u} \cdot t + \frac{1}{2} \cdot \bar{a} \cdot t^2 \text{ (meter)} \tag{4.23}$$

where,

s = displacement of the particle clusters at a time 't',

u = initial velocity of the magnetic particle clusters,

The density of iron is 7970 kilogram per cubic meter in the SI system. Also as mentioned earlier the size of the particles is in the order of microns. Since the number of particles can be very large, it is computationally expensive to compute the mass of each particle independently. Rather, an average size can be assumed for the particles. In this model, the diameter of the particles is assumed to be 1 micron. The volume 'V' and the mass 'm' of the particle can be calculated according to

$$V = \frac{4}{3} \cdot \pi \cdot (\frac{dia}{2})^3 \quad \text{(cubic meter)} \tag{4.24}$$

where,

dia = diameter of the particles (in meter),

π = 3.142 (approximately).

$$m = V \cdot \rho \quad \text{(kilograms)} \tag{4.25}$$

where,

ρ = density of iron (in kilogram per cubic meter).

The saturation magnetization of iron is 1.7×10^6 Ampere per meter. The magnetic dipole moment 'M' is thus

$$M = mag \cdot V \quad \text{(Ampere - sq. meter)} \tag{4.26}$$

where,

mag = saturation magnetization (in Ampere per meter).

This is valid because of the tri-state assumption for the magnetic particles. The gradient of the magnetic field is found by the first order Taylor series approximation for the gradient of a continuous function which is shown in equation (4.27).

$$\frac{\partial H}{\partial d} = \frac{H_2 - H_1}{d_2 - d_1} \tag{4.27}$$

where,

H_1, H_2 = fields at the location d_1 and d_2 respectively.

Parameters for quantitative analysis of the MPI method

The MPI model developed so far can generate a sequence of MPI image matrices which can be used for a quantitative analysis of the specimen under test. However for automatic processing of data in the MPI images, mathematical features of the image need to be defined which contain all the relevant information in the image. This also reduces memory requirements for data processing. The selected features of the MPI images are "efficiency", "time to equilibrium" [1] and the "signal to noise ratio".

The time to equilibrium is the observation time for which the relation in equation (4.28) holds.

$$(\sum_{i=c}^{d}\sum_{j=e}^{f} m_c)_{te} = (\sum_{i=c}^{d}\sum_{j=e}^{f} m_c)_{te+x} \tag{4.28}$$

where,

te = time to equilibrium,

x = any positive real number,

c..d, e..f = the matrix coordinates corresponding to the location of the flaw as shown in Figure 4.7.

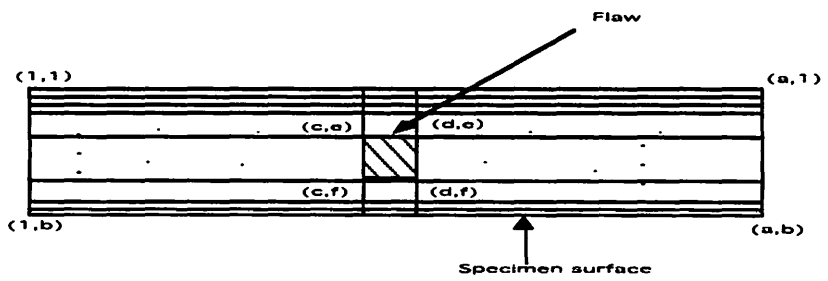

Figure 4.7. Co-ordinates of the location of the flaw

Thus the time to equilibrium is the minimum time of observation after which the MPI image matrix does not change in the neighborhood of the flaw. This image matrix contains the output data which can be processed for detection of discontinuities. Any image matrix recorded before 'te' contains incomplete data.

The mathematical expression for the efficiency is given in equation (4.29)

$$\text{efficiency} = \frac{(\sum_{i=c}^{d}\sum_{j=e}^{f} m_c)_{te}}{(\sum_{i=1}^{a}\sum_{j=1}^{b} m_c)_{t_0}} \tag{4.29}$$

and the expression for the signal to noise ratio is given by equation (4.30)

$$\text{SNR} = \frac{(\sum_{i=c}^{d}\sum_{j=e}^{f} m_c)_{te}}{(\sum_{i=1}^{a}\sum_{j=1}^{b} m_c)_{te} - (\sum_{i=c}^{d}\sum_{j=e}^{f} m_c)_{te}} \tag{4.30}$$

where,

t_0 = start time of observation,

SNR = signal to noise ratio.

The relevance of these features for MPI image characterization is significant. This is because there exists a large leakage field in test specimens due to edge effects. As a result not all particles sprayed are attracted to the flaw. Some are forced off the surface while some are held in the background giving rise to noise. The efficiency gives an estimate of the number of particles which give an indication of the flaw while the signal to noise ratio gives the strength of the defect indication relative to the background noise.

The simulation algorithm

The discretization used to model the MPI testing process is suitable for computer simulations of the model. The overall algorithm is summarized below [1]. High level languages such as C, PASCAL, FORTRAN etc. or mathematical packages such as MATLAB can be

used to realize the algorithm.

1. The total number of magnetic particles sprayed is specified by the user as a function of the required intensity and the size of the specimen.

2. The particle distribution on the surface of the specimen is generated using the statistical model.

3. The finite element model is solved to obtain the leakage fields on the surface of the specimen for given boundary conditions.

4. The forces on the magnetic particle clusters are calculated along with their corresponding accelerations using the force model.

5. For each cluster, the displacement is calculated by a flow chart shown in Figure 4.8

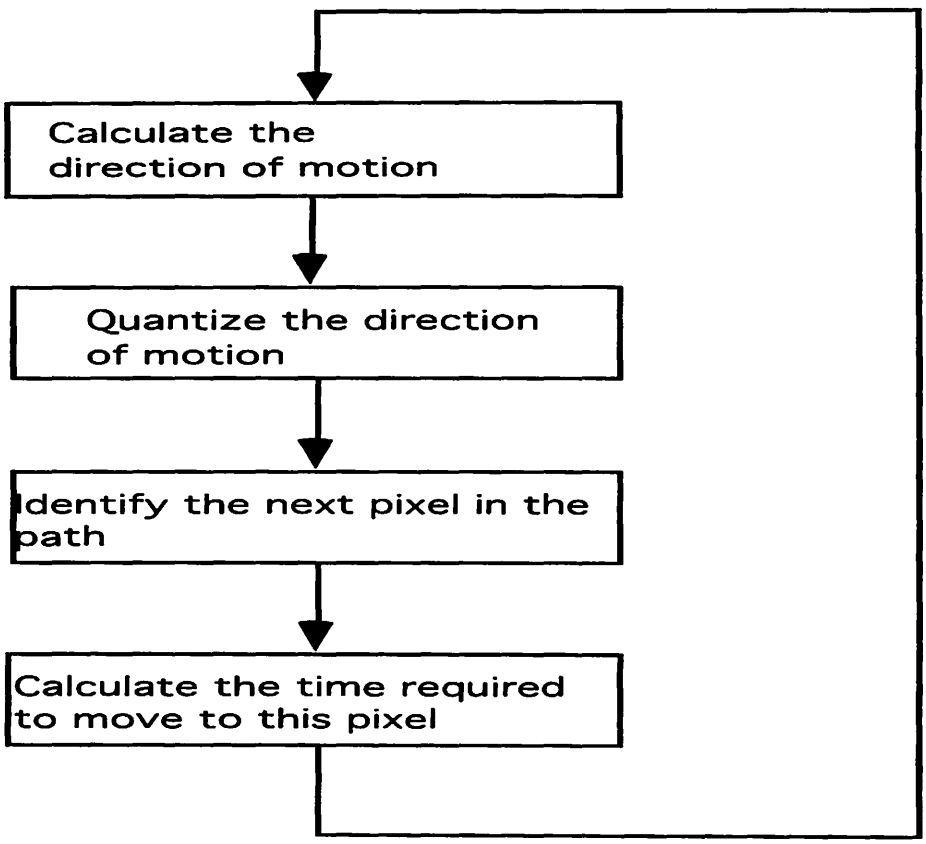

Figure 4.8. Flowchart for calculating displacements of particles

This is repeated until the following termination criteria are met

a. The particle reached the flaw.

b. The particle migrated out of the region of interest.

6. The time for observation is selected.

7. The corresponding position data of the magnetic particles is extracted from step (5). This information is translated into particle density to generate MPI images.

8. The time to equilibrium of the magnetic clusters and the efficiency of the MPI method is calculated.

CHAPTER 5. FLAW CHARACTERIZATION STUDIES

Description of the test specimen

The results of simulating the overall model are presented in this chapter. A rectangular block of 0.1 percent carbon steel was modeled. The dimensions of the block are 10.16 cm. x 5.08 cm. x 2.54 cm. The density of the block is 7835 kilogram per cubic meter and its elastic modulus is 21.48 x 10^4 MPa. A rectangular discontinuity due to metal loss is present at the center of its upper face. The dimensions of the discontinuity are 0.05 cm. x 1.27 cm. x 0.8 cm. The material of the discontinuity is air as the discontinuity is a metal loss defect. Figure 5.1 shows the dimensions of the test specimen while Figures 5.2 and 5.3 show the B/H curves of the specimen and the discontinuity respectively.

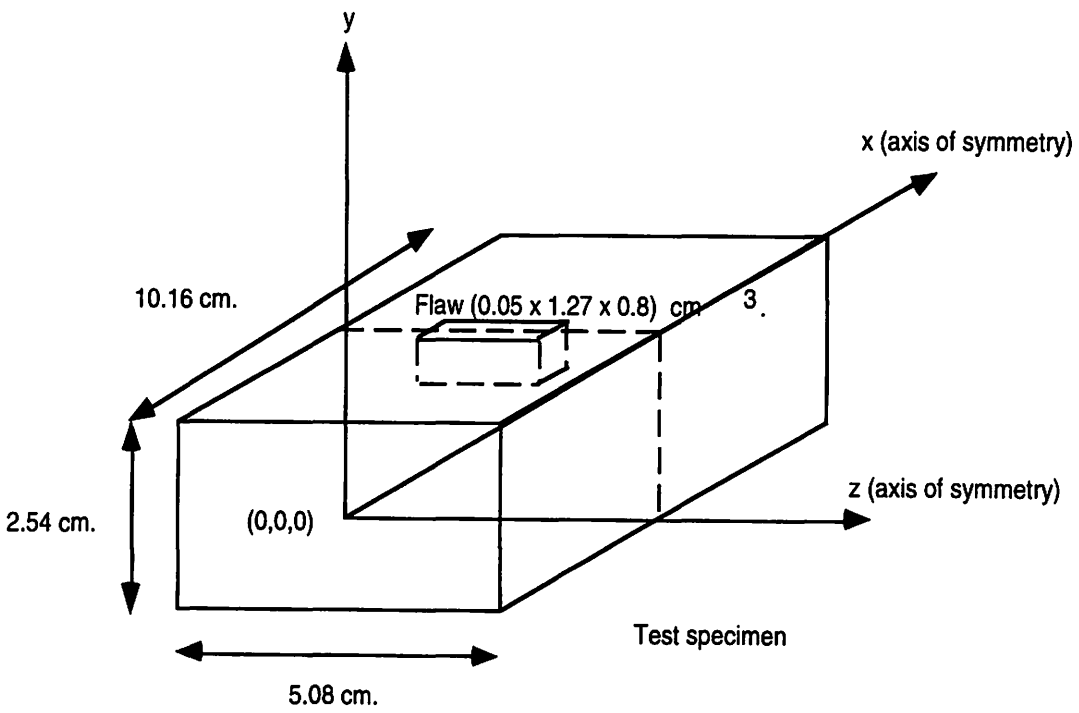

Figure 5.1. The test specimen

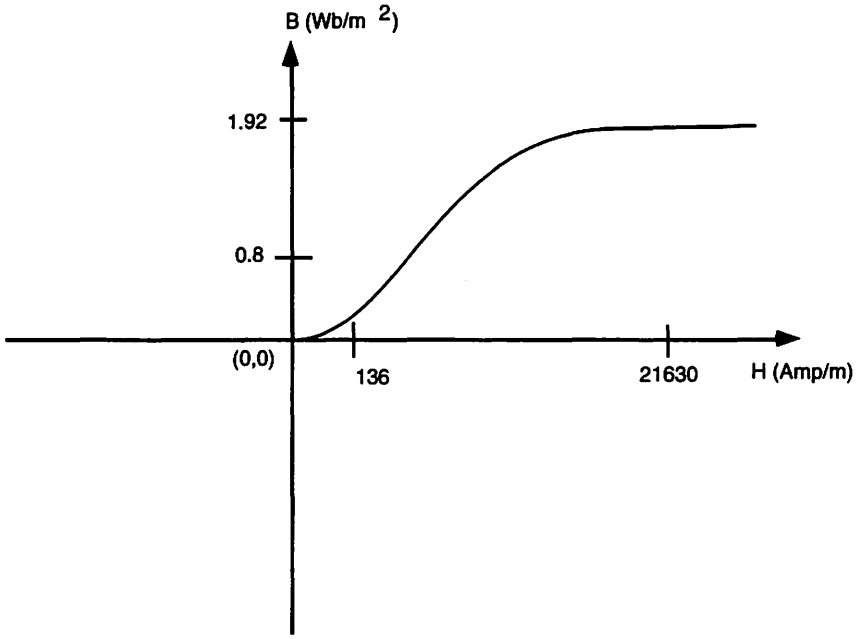

Figure 5.2. Magnetization curve of the test specimen

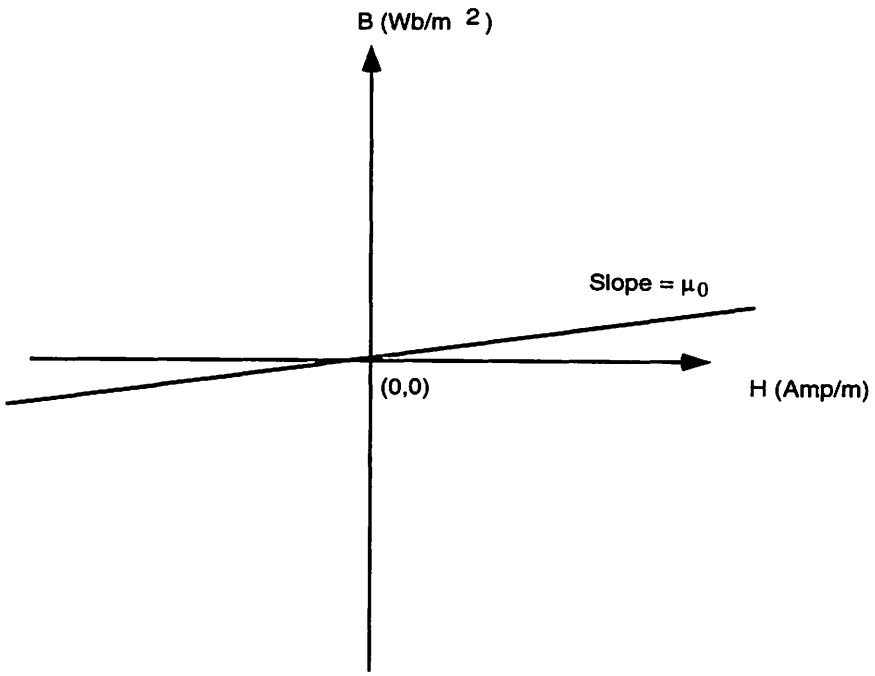

Figure 5.3. Magnetization curve of the discontinuity

MPI images

The specimen is energized by an electromagnet such that longitudinal magnetization is applied to its faces in the y - z plane. This is supplied as the boundary condition to the three dimensional finite element model. The specimen is symmetric about two of its axes as depicted in Figure 5.1. Hence only one quarter of the specimen is modeled to reduce the computational complexity [24] [25]. This is displayed in Figure 5.4.

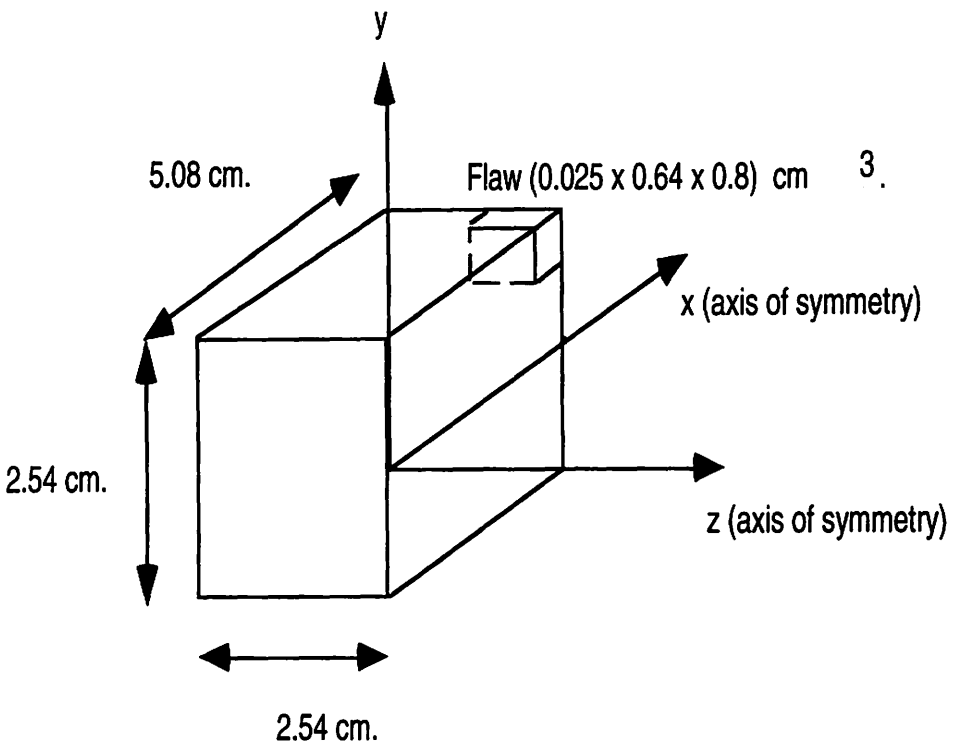

Figure 5.4. The quarter geometry of the specimen

All computations of the statistical model and the force model are also carried out on the quarter geometry of the specimen taking advantage of its symmetry. With a boundary condition of 1.4 Tesla, the leakage field signals were obtained using the ELM. Their distribution on the entire surface is shown in Figure 5.5, Figure 5.6 and Figure 5.7 [24].

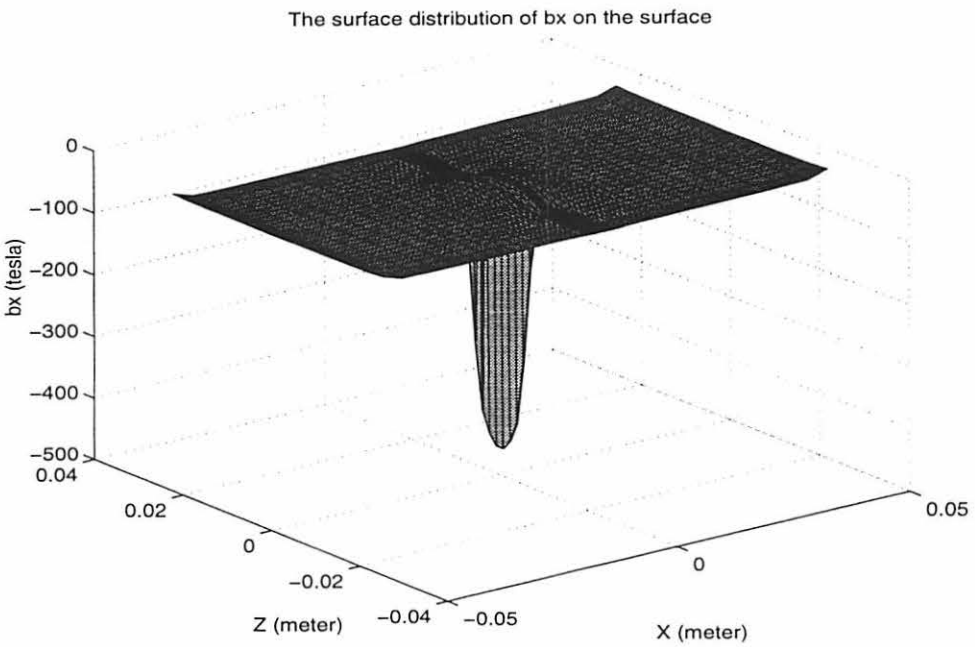

Figure 5.5. The component of the leakage field measured along the x axis

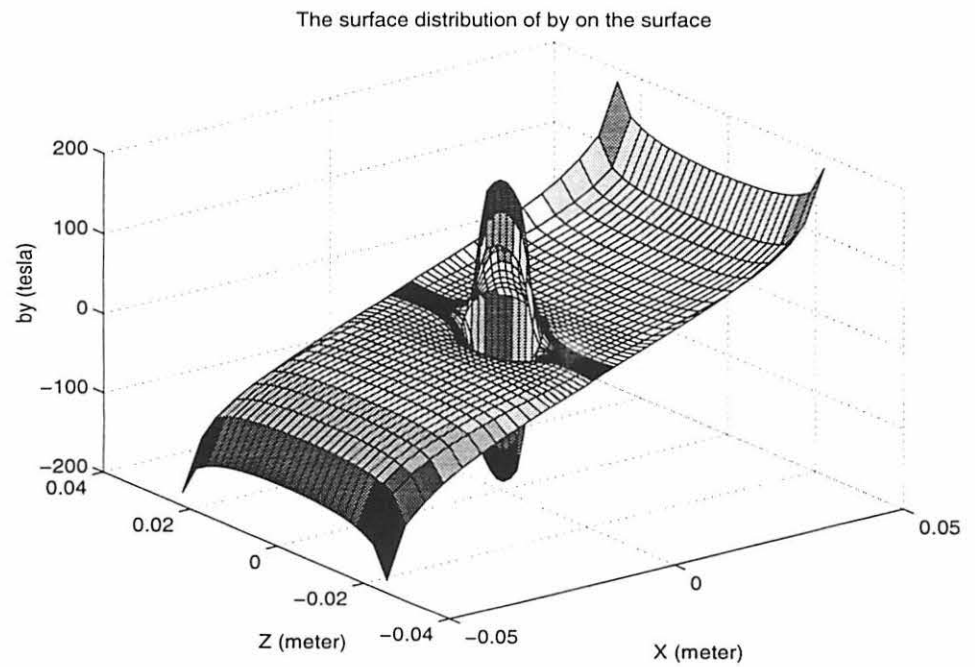

Figure 5.6. The component of the leakage field measured along the y axis

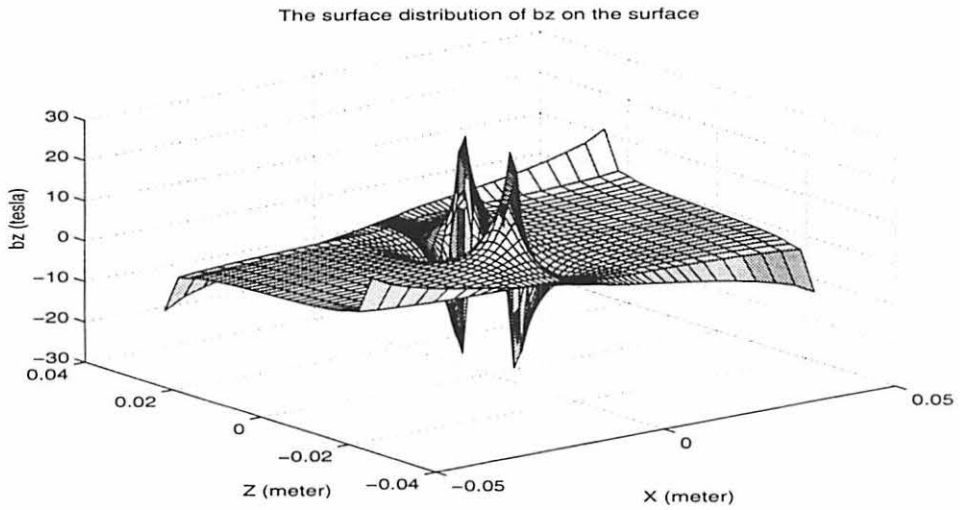

Figure 5.7. The component of the leakage field measured along the z axis

These leakage field signals induce a force on the magnetic particles. The force and the acceleration are computed by the force model. The distribution of the components of the force along the x and the z axes and the corresponding accelerations of the magnetic particles on the entire surface are depicted in Figures 5.8, 5.9, 5.10, and 5.11 [1].

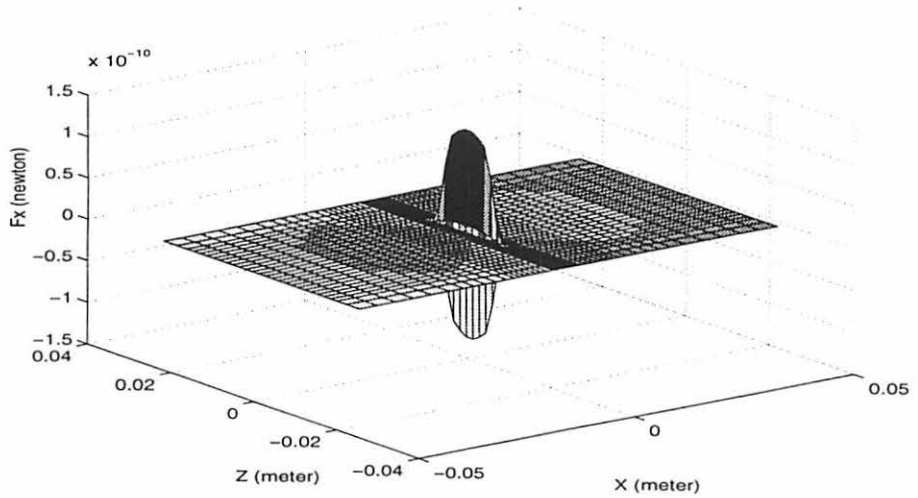

Figure 5.8. The surface distribution of the component of the force along the x axis

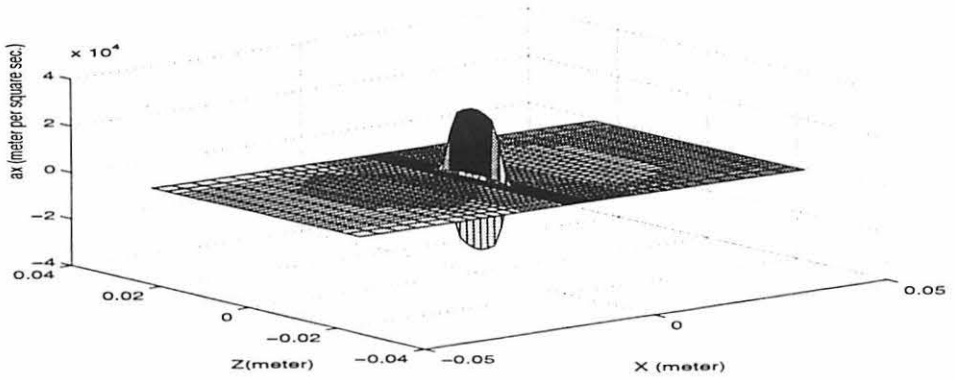

Figure 5.9. The surface distribution of the component of acceleration along the x axis

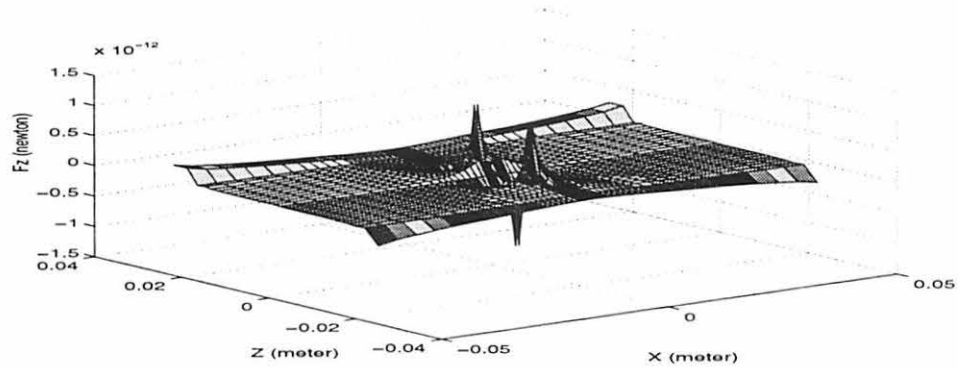

Figure 5.10. The surface distribution of the component of force along the z axis

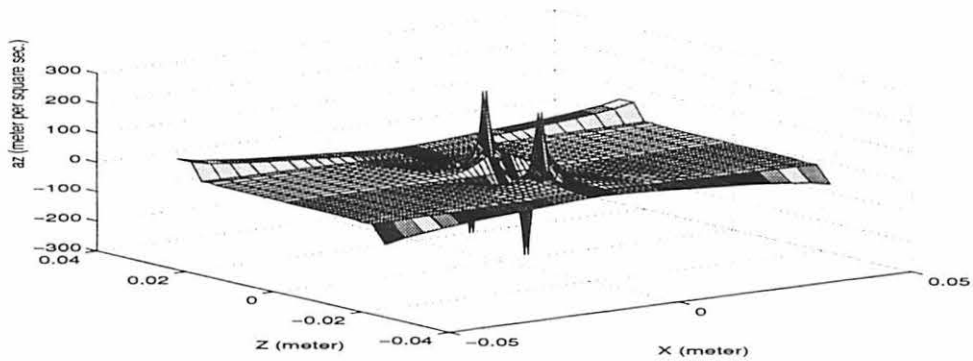

Figure 5.11. The surface distribution of the component of acceleration along the z axis

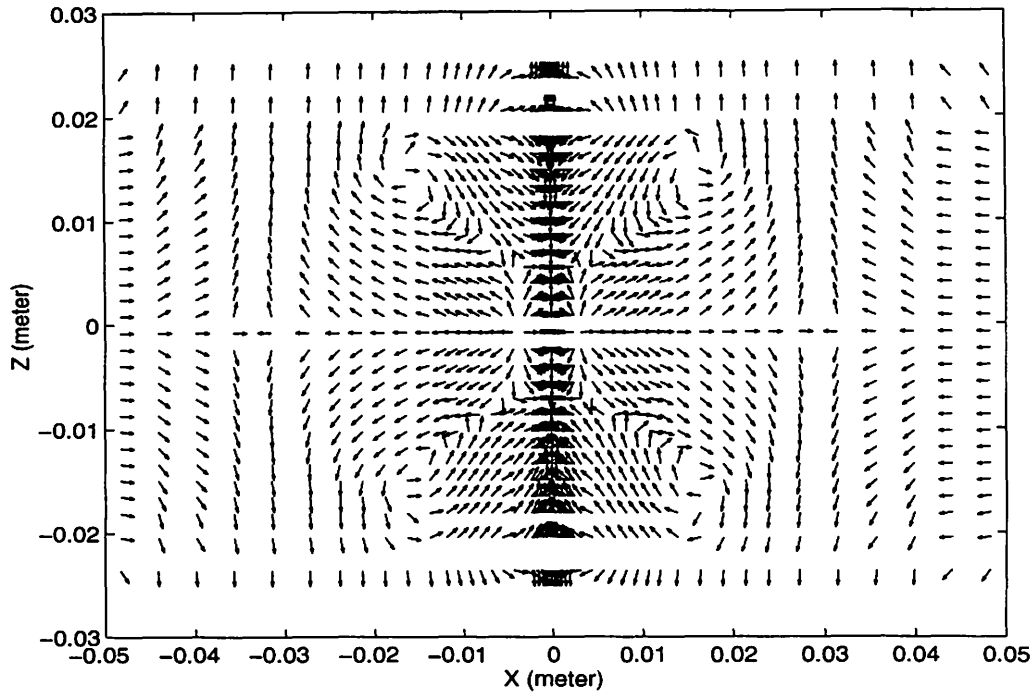

Figure 5.12. The direction of motion of magnetic particles

The motion of the particles is in a plane which is perpendicular to the surface of the earth. Hence the effect of the gravitational force on the particles is neglected. Similarly, the component of the magnetic force along the y - axis has no effect on their motion.

The displacement of the particle clusters depends on their initial position on the surface of the test specimen. Particle clusters close to the edge experience a force which drives them off the surface. Other particle clusters move towards the flaw. Images of the path of some of the particle clusters are displayed in Figures 5.13, 5.14 and 5.15. In these figures only one quarter of the geometry is displayed. The flaw is present at the lower right hand corner of the image. Figure 5.13 shows an path of a particle cluster from its initial location at (-0.025, -0.015) which falls into the flaw. Figure 5.14 shows the path of a particle from its initial position at (-0.035, -0.02) which goes off the surface. Figure 5.15 shows the path of another particle which starts at location (-0.04, -0.01) and falls into the flaw.

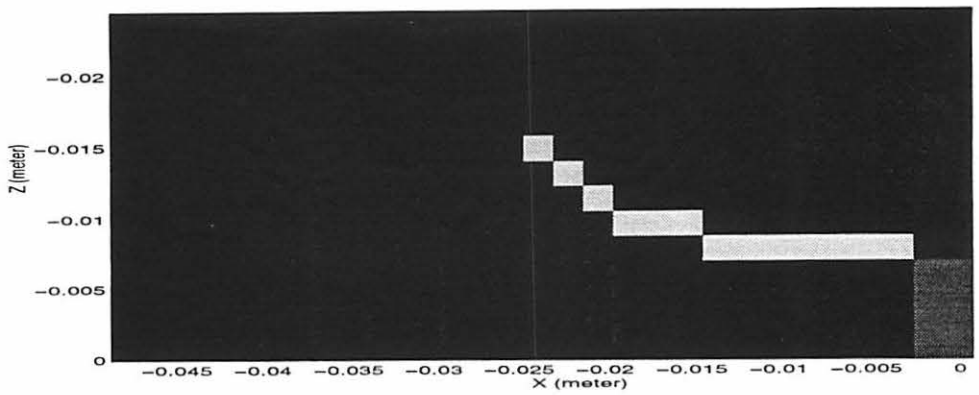

Figure 5.13. Sample path of a particle cluster moving towards the flaw

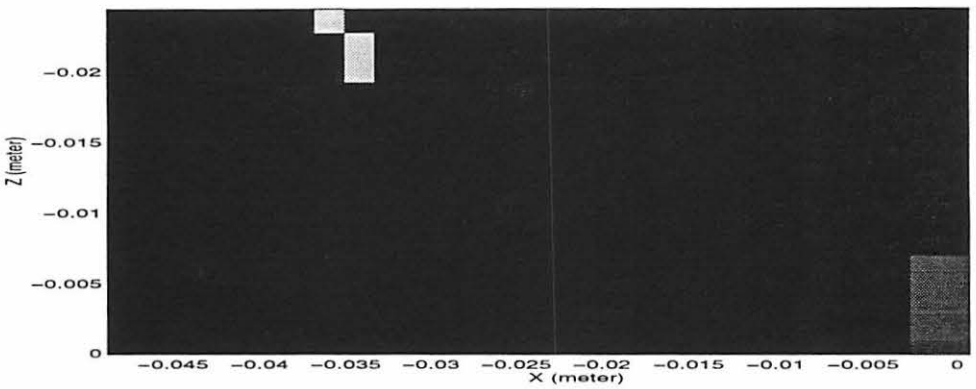

Figure 5.14. Sample path of another particle cluster which falls off the surface

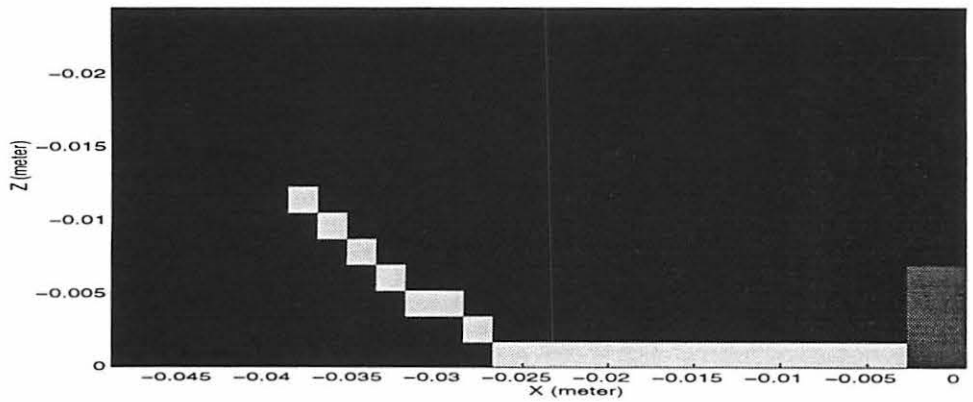

Figure 5.15. Sample path of a particle cluster which moves towards the flaw

The images of the mass matrix at different observation times are displayed in Figures 5.16, 5.17, 5.18, 5.19, 5.20, 5.21 and 5.22 [1]. The gray level intensity is normalized to map the maximum value in the matrix to a gray level of eight. It can be seen clearly that the mass matrix changes rapidly to indicate the accumulation of the particles around the flaw in 0.6 seconds. The discontinuity is thereby detected effectively.

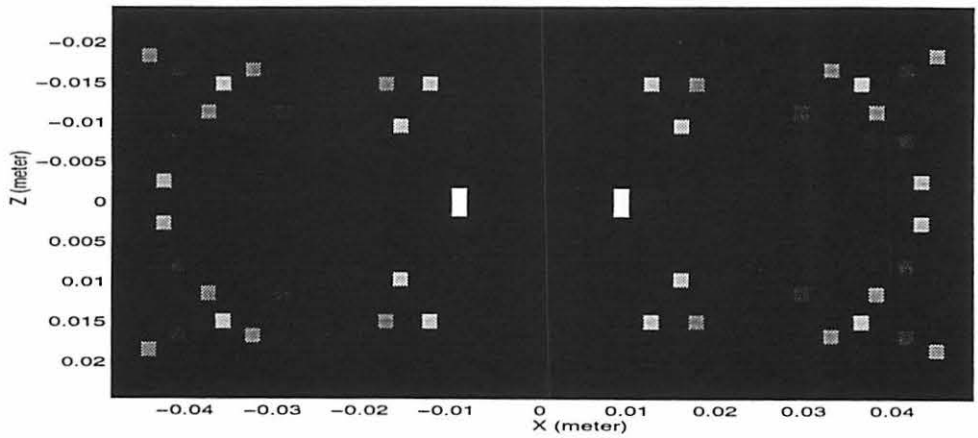

Figure 5.16. The image of the mass matrix at t = 0 seconds

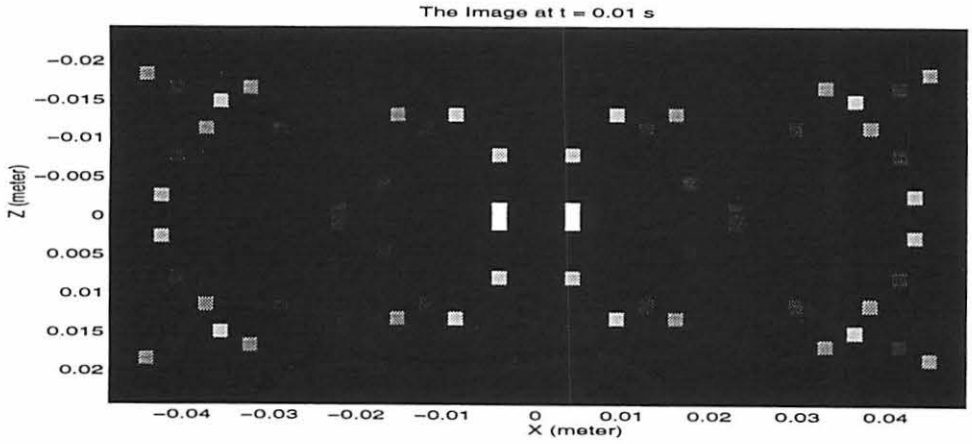

Figure 5.17. The image of the mass matrix at t = 0.01 seconds

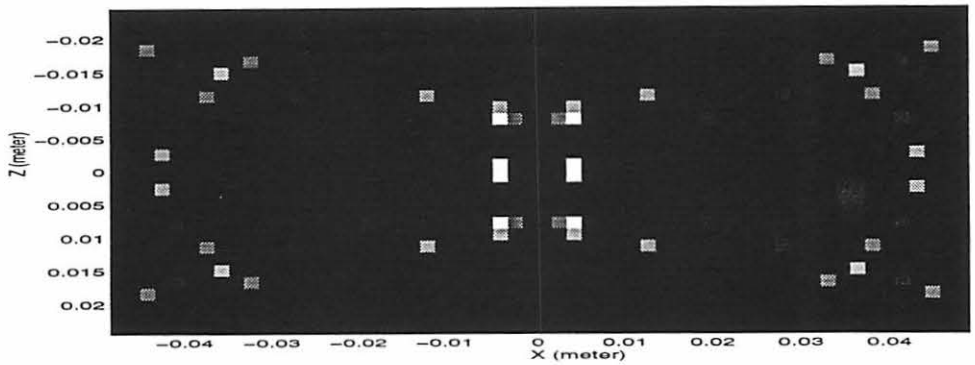

Figure 5.18. The image of the mass matrix at t = 0.02 seconds

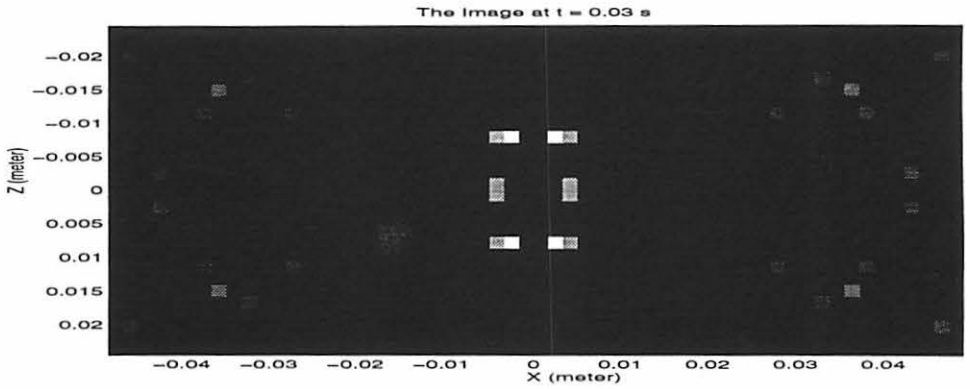

Figure 5.19. The image of the mass matrix at t = 0.03 seconds

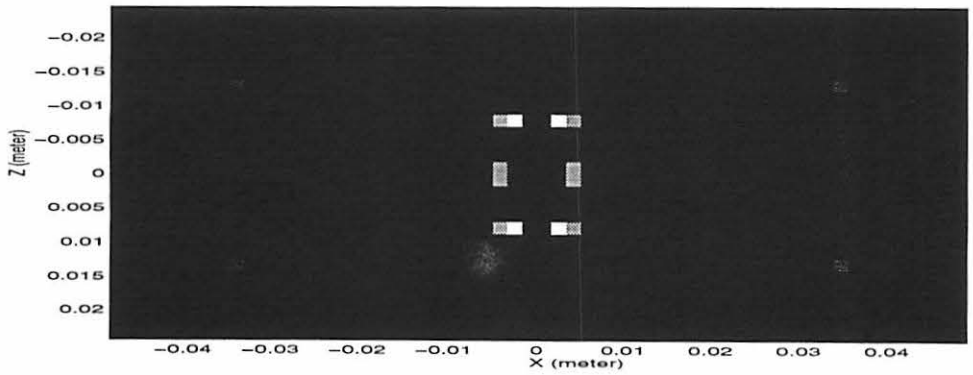

Figure 5.20. The image of the mass matrix at t = 0.08 seconds

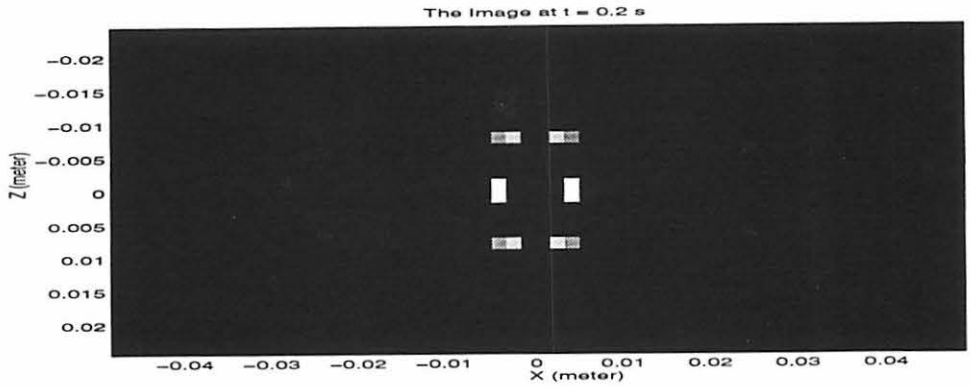

Figure 5.21. The image of the mass matrix at t = 0.2 seconds

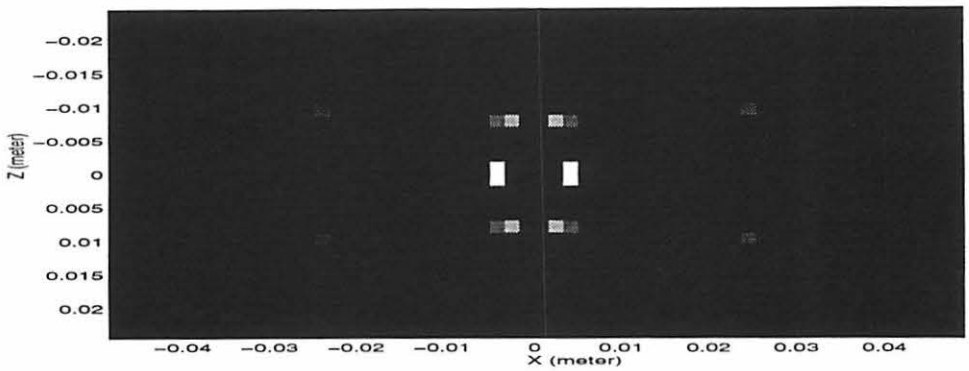

Figure 5.22. The image of the mass matrix at t = 0.6 seconds

It is noticed that the flaw images have distinct dark gaps between regions of high intensity. The high intensity pixels correspond to regions of high particle concentration while the dark gaps correspond to the absence of these particles. This occurrence is attributed to the discretization of the specimen surface into a finite number of pixels. Further the motion of the particles is normalized in eight directions which forces the particle clusters to move along the grid of the pixel centroids. A finer discretization mesh will eliminate the problem and provide a more continuous indication of the flaw.

Parametric studies and discussion

The MPI model can be used to obtain optimum experimental conditions for the specimen under test. This is achieved by conducting several simulations for different values of the input energy in the form of boundary condition of the flux density for the three dimensional finite element model. The width and the length of the flaw are chosen as 0.05 cm. and 1.27 cm. respectively. However the flaw depth is varied from 10 percent to 50 percent of the thickness of the specimen. The parameters under study are the efficiency, time to equilibrium for the corresponding efficiency and the signal to noise ratio. Table 5.1 shows the results of the efficiency of the MPI method for various magnetization levels and flaw depths.

Table 5.1. Efficiency of the MPI method

	Flaw depth (cm.)				
Flux density (Tesla)	0.254	0.508	0.762	1.106	1.270
0.25	0.46	0.42	0.38	0.38	0.37
0.5	0.37	0.39	0.33	0.33	0.32
0.75	0.3	0.32	0.45	0.43	0.41
1.0	0.54	0.64	0.7	0.71	0.74
1.25	0.42	0.53	0.54	0.54	0.58
1.5	0.2	0.33	0.34	0.38	0.4
1.75	0.2	0.21	0.21	0.23	0.41
2.0	0.16	0.18	0.2	0.23	0.25

Figure 5.23 displays the variation of the efficiency with the input magnetization level for various flaw depths. It is seen that the efficiency for any flaw depth shows a distinct peak around 1 Tesla. This value of the flux density lies in the middle of the linear region of the B-H curve of the specimen. As the input magnetization increases beyond 1 Tesla, the efficiency falls. This is due to the fact that there exist two dominant magnetic forces on the surface of the test specimen. The first component is due to the leakage field around the flaw and the other is due to the leakage field at the specimen edges. These two forces oppose each other and the final distribution of the particles is influenced by their relative strengths and the initial distribution of particles. Increasing the flaw depth and magnetization level results in an increase of the force due to the leakage field of the flaw. However, the edge effect also increases since most of the test specimen gets saturated at higher magnetization levels. The B-H curve of the specimen influences the proportion of increase in the magnitude of each force. The results shown are thus specific to the size, shape and material properties of the test specimen.

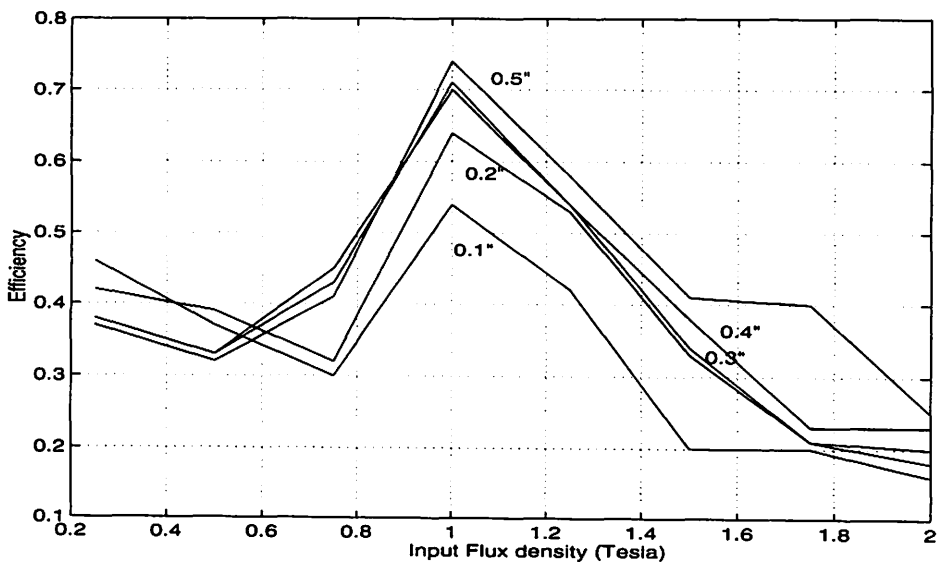

Figure 5.23. Variation of efficiency for different flaw depths

The time to equilibrium for the corresponding efficiency decreases with increasing flaw depths and with increase in the values of the input magnetization. The values of the time to equilibrium for various input magnetization levels and flaw depths are tabulated in Table 5.2

Table 5.2. The time to equilibrium for the corresponding efficiency

	Flaw depth (cm.)				
Flux density (Tesla)	0.254	0.508	0.762	1.106	1.270
0.25	0.806	1.219	0.448	0.556	0.597
0.5	0.621	0.616	0.662	0.649	0.632
0.75	0.777	0.718	0.589	0.553	0.846
1.0	1.182	0.748	0.604	0.527	0.503
1.25	0.620	0.503	0.423	0.588	0.441
1.5	0.336	0.229	0.354	0.291	0.413
1.75	0.184	0.146	0.178	0.226	0.306
2.0	0.167	0.132	0.231	0.217	0.166

Figure 5.24 shows a graphical representation of Table 5.2. The decrease in the value of the time to equilibrium with increasing flux density is not monotonous. This is because of two reasons. One of the reasons is the disproportionate increase in the values of the two forces discussed previously. The other reason is that some particles oscillate between two

grid points of opposite gradients affecting the measured value of this parameter. The largest value of this parameter is 1.219 seconds while the smallest value is 0.166 seconds. This can be used to design the speed of the imaging system used in the MPI method. From the results obtained it is clear that the imaging system must operate at a frequency less than 0.82 Hz if only the final image is desired. However if a large number of image samples are required the imaging system must operate at a frequency greater than 6.02 Hz.

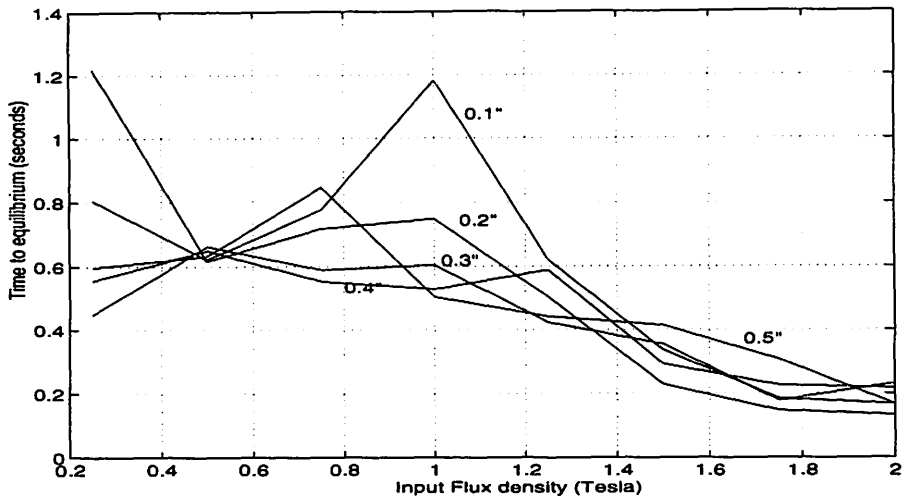

Figure 5.24. Variation of time to equilibrium for different flaw depths

The signal to noise ratio represents the effect of background noise on the probability of detection. The background is obtained primarily due to particle clusters which oscillate about their initial position These clusters are under the influence of forces which neither drive them close to the flaw nor off the specimen surface. It follows the same trend as the efficiency and becomes infinite at 1 Tesla for a flaw depth of 1.27 cm. This is shown in Table 5.3. Figure 5.25 shows a graphical display of Table 5.3. The infinite value in one of the columns of Table 5.3 is not shown explicitly. Rather it is represented by two parallel lines, the intersection of which is theoretically at infinity.

Table 5.3. Variation of the signal to noise ratio

	Flaw depth (cm.)				
Flux density (Tesla)	0.254	0.508	0.762	1.106	1.270
0.25	1.21	1.02	0.9	0.9	0.88
0.5	0.97	1.1	0.82	0.76	0.75
0.75	0.75	0.88	1.64	1.38	1.28
1.0	4.26	8.43	19.92	23.58	Inf.
1.25	1.86	2.0	2.33	2.62	3.44
1.5	0.36	0.78	0.83	0.86	0.92
1.75	0.32	0.32	0.32	0.35	0.85
2.0	0.23	0.25	0.3	0.33	0.36

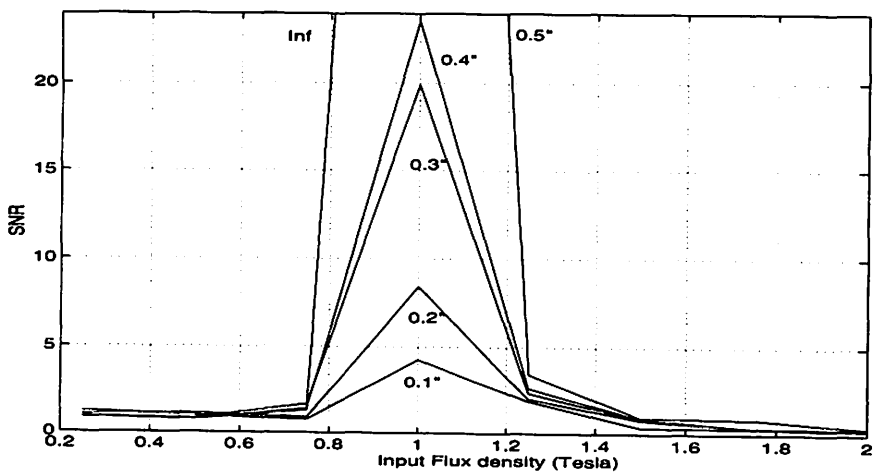

Figure 5.25. Variation of signal to noise ratio for different flaw depths

The parameters discussed give tremendous information regarding the MPI method. One useful result is the optimum experimental condition in terms of input flux density for the test specimen. From Figures 5.23, 5.24, and 5.25 it is clear that maximum efficiency and signal to noise ratio is obtained in the neighborhood of 1 Tesla.

CHAPTER 6. CONCLUSION

Conclusions

Electromagnetic NDE methods are extensively used in heavy metal industries due to the sensitivity of metals to electromagnetic energy in the whole spectrum. The magnetic particle inspection (MPI) method derives its name from the use of magnetic particles as sensors in a popular electromagnetic method called the magnetic flux leakage (MFL) method. The MPI method has been in use since the early 1920s, however the method has remained largely qualitative due to lack of quantitative modeling efforts. This thesis provides a quantitative insight into the complex physics underlying the MPI method. It is the first attempt to explain the particle dynamics using imaging techniques.

The entire MPI process is broken into three discrete steps and models are developed for each step. A statistical model simulates the initial distribution of particles under the assumption that the specimen does not possess any residual magnetism. The three dimensional linear finite element model predicts the leakage field on the surface of the specimen in the presence of a flaw and applied magnetic field. The force model calculates the displacements of the particles by quantifying the force and acceleration experienced by them.

The MPI method involves the use of millions of particles and hence the precise modeling of the behavior of every particle is computationally expensive. The proposed simulation model makes the computational complexity independent of the number of particles by discretizing the specimen surface into pixels and mapping the particles onto the pixels themselves. The accuracy of the model is directly proportional to the density of the mesh as is the computational complexity. The mesh used tries to achieve an equilibrium between these contradictory requirements.

The modeling information is encoded into two matrices viz. the mass matrix and the

moment matrix, the sizes of which are equal to the mesh discretization used. Imaging techniques are then applied to these matrices to obtain a visual picture of the particle behavior. The dynamics of the particles is recreated at a speed perceivable to the human eye.

The proposed approach is capable of generating MPI flaw images. This helps to define features such as the time to equilibrium of the magnetic particles, efficiency and signal to noise ratio of the MPI image. Optimum experimental conditions are then obtained by conducting several simulations of the model for different values of input energy and depths of the flaw.

Image features such as the time to equilibrium and the efficiency further reduce the memory requirements and help in parametric studies of the MPI method. Simulations using the MPI model indicate that the time to equilibrium for the corresponding efficiency decreases with increasing flaw depth and increasing values of the input energy. The values range from 0.1662 to 1.219 seconds. The efficiency of the method shows a maximum for a boundary condition of 1 Tesla for any flaw depth. Since the sampling used for simulation is 0.25 Tesla it can be reliably said that the maximum efficiency lies between 0.75 and 1.25 Tesla. These values can be claimed as the optimum boundary conditions for the specimen under test. The signal to noise ratio follows the same trend as the efficiency. Its values range from 0.23 to infinity. This parameter is critical for the detection of the flaw as it indicates the effect of background noise on the detection capability.

The model predictions are affected by the approximations made during its formulation. Some significant assumptions are the elimination of viscous, interparticle etc. forces, lack of the residual magnetism in the specimen, and a tri-state assumption of the particle permeabilities. However the results obtained agree with intuitive reasoning establishing the validity of the model.

The simulated data can be used to design an electromagnetic NDE system capable of

classifying test objects. Algorithms such as neighborhood processing, adjacent cell linking etc. can be used to analyze the image data obtained from the simulation model. These algorithms are well suited for a digital computer. The optimization of the test parameters can increase the probability of detection of the flaw significantly.

Recommendations for future research

The model assumes that the specimen is initially unmagnetized. The presence of remnant magnetism can be included as initial conditions to the statistical and finite element models to predict the distribution of particles and fields respectively. The remnant fields will result in a biased distribution of the particles and a different B-H curve will have to be used for the finite element model.

The accuracy of the model can be improved however little by taking into account the effects of viscous and interparticle forces. The mesh density can be optimized by analytical techniques or through simulations using the model.

Features apart from the efficiency and the time to equilibrium can be defined to better characterize the MPI flaw images. An automatic electromagnetic NDE system can be constructed by using the image data along with a digital computer employing algorithms such as neighborhood processing or adjacent cell linking.

The POD concept can be incorporated into the MPI model. The variability used can be the initial distribution of particles and their luminosity. Other human visualization factors can also be modeled to make the probability calculations accurate.

The model solves the forward modeling problem of predicting the dynamics of the magnetic particles under the assumption of a known flaw. The transfer functions of the parameters obtained can be used to solve the inverse problem of calculating the flaw dimensions from the dynamic behavior of the particles.

BIBLIOGRAPHY

[1] Atul S. Athavale, L. Udpa, S. S. Udpa and Zuorong Zhang. *MPI Simulation Model for Nondestructive Evaluation*, Review of Progress in QNDE, Plenum Press, New York, 1995 (in press).

[2] R. E. Beissner and M. J. Sablik. *Flaw Characterization by the Magnetic Leakage Field Method*, Final report, SWRI Project 15-9248, Mar. 1983, pp 13-46.

[3] A. P. Berens and P. W. Hovey. *Statistical Methods for Estimating Crack Detection Probabilities*, Probabilistic Fracture Mechanics and Fatigue Methods: Applications for Structural Design and Maintenance, STP 798, J. M. Bloom and J. C. Ekvall. Ed., American Society for Testing and Materials, Chicago, 1983, pp 79-84.

[4] C. E. Betz. *Principles of Magnetic Particle Testing*, 1st ed., Magnaflux Corp., Chicago, Feb. 1967.

[5] K. J. Binns, M. A. Jabbar and W. W. Barnard. *Computation of the Magnetic Field of Permanent Magnets in Iron Cores*, Proc. of the IEEE, Vol. 122, No. 12, Dec. 1975, pp 1377-1381.

[6] P. J. Blackley, J. Simkin, S. T. Brown. *Validation of Finite Element Analysis of the Magnetic Fields around Cracks*, IEEE Transactions on Magnetics, Vol. MAG-21, No. 6, Nov. 1985, pp 2420 - 2423.

[7] D. E. Bray and R. K. Stanley. *Nondestructive Evaluation*, McGraw Hill, New York, 1989.

[8] William Hayt. *Engineering Electromagnetics*, McGraw Hill, New York, 1981

[9] J. H. Hwang and W. Lord. *Magnetic Leakage Field Signatures of Material Discontinuities*, Proceedings of the Tenth Symposium on Nondestructive Evaluation, San Antonio, April 1975, pp 13-46.

[10] D. C. Jiles. *Introduction to Magnetism and Magnetic Materials*, 1st ed., Chapman and Hall, London, 1991.

[11] W. Lord and J. H. Hwang. *Defect Characterization from Magnetic Leakage Fields*, British Journal of NDT, Vol 19, No. 1, Jan. 1977, pp 14-18.

[12] Robert C. McMaster, Paul McIntire and Michael L. Mester. *Nondestructive Testing Handbook*, Second Ed., Vol. 4, Electromagnetic Testing, ASNT, USA, 1986.

[13] L. A. Pars. *An Introduction to Calculus of Variations*, Heineman, London, 1962.

[14] S. N. Rajesh, L. Udpa, S. S. Udpa. *Numerical Model Based Approach for Estimating Probability of Detection in NDE Applications*, IEEE Conference of Electromagnetic Field Computation, June 1992, pp 385-395.

[15] L. J. Segerlind. *Applied Finite Element Analysis*, John Wiley and Sons Ltd., New York, 1976.

[16] P. Silvester and M. V. Chari. *Finite Element Solutions of Saturable Magnetic Field Problems*, IEEE Transactions on Power Apparatus and Systems, Vol. PAS-90, No. 2, March 1971, pp 168-175.

[17] G. Subramanya, L. Udpa and S. S. Udpa. *Probability of Detection Model for Magnetostatic Nondestructive Evaluation*, Proceedings of the 3rd Annual Midwest Electro-technology Conference, pp 47-50, April 1994.

[18] G. Subramanya. *Probability of Detection Model for Nondestructive Evaluation*, MS Thesis, Iowa State University, Ames, Summer 1994.

[19] J. Thomas, Kermit Skeie and Paul McIntire. *Nondestructive Testing Handbook*, Second Ed., Vol. 6, Magnetic Particle Testing, ASNT, USA, 1989.

[20] J. F. Traub. *Iterative Methods for the Solution of Equations*, Prentice Hall, Englewood Cliffs, N. J. 1964.

[21] S. S. Udpa, W. Lord and Y. S. Sun. *Numerical Modeling of Residual Magnetic Phenomena*, IEEE Transactions on Magnetics, Vol. MAG-21, No. 6, Nov. 1985, pp 2165-2168.

[22] W. C. Yen. *Finite Element Characterization of Residual Fields*, MS Thesis, Colorado State University, Fort Collins, Fall 1978.

[23] O. C. Zeinkiewicz. *The Finite Element Method In Engineering Science*, McGraw Hill, London, 1971.

[24] Zuorong Zhang et al. *An Equivalent Linear Model for Magnetostatic Nondestructive Evaluation*, IEEE Transactions, June 1996 (in press).

[25] Zuorong Zhang, L. Udpa, S. S. Udpa and Atul Athavale. *Linearized MFL Model for Embedded Flaw Detection in Rails*, Review of Progress in QNDE, Plenum Press, 1995 (in press).